1978

Production of ultra low frequency magnetic noise by ocean surface gravity waves and its real time removal from airborne magnetometer measurements.

Etro, James Francis

Monterey, California. Naval Postgraduate School

NAVAL POSTGRADUATE SCHOOL
Monterey, California

THESIS

PRODUCTION OF ULTRA LOW FREQUENCY MAGNETIC NOISE BY OCEAN SURFACE GRAVITY WAVES AND ITS REAL TIME REMOVAL FROM AIRBORNE MAGNETOMETER MEASUREMENTS

by

James Francis Etro

December 1978

Thesis Advisor: A. B. Chace

Approved for public release; distribution unlimited.

SECURITY CLASSIFICATION OF THIS PAGE (When Data Entered)

REPORT DOCUMENTATION PAGE

READ INSTRUCTIONS BEFORE COMPLETING FORM

1. REPORT NUMBER	2. GOVT ACCESSION NO. / 3. RECIPIENT'S CATALOG NUMBER
4. TITLE (and Subtitle) Production of Ultra Low Frequency Magnetic Noise by Ocean Surface Gravity Waves and Its Real Time Removal From Airborne Magnetometer Measurements	5. TYPE OF REPORT & PERIOD COVERED: Master's Thesis; December 1978
	6. PERFORMING ORG. REPORT NUMBER
7. AUTHOR(s): James Francis Etro	8. CONTRACT OR GRANT NUMBER(s)
9. PERFORMING ORGANIZATION NAME AND ADDRESS: Naval Postgraduate School, Monterey, CA 93940	10. PROGRAM ELEMENT, PROJECT, TASK AREA & WORK UNIT NUMBERS
11. CONTROLLING OFFICE NAME AND ADDRESS: Naval Postgraduate School, Monterey, CA 93940	12. REPORT DATE: December 1978
	13. NUMBER OF PAGES: 71
14. MONITORING AGENCY NAME & ADDRESS (if different from Controlling Office): Naval Postgraduate School, Monterey, CA 93940	15. SECURITY CLASS. (of this report): Unclassified
	15a. DECLASSIFICATION/DOWNGRADING SCHEDULE

16. DISTRIBUTION STATEMENT (of this Report)

Approved for public release; distribution unlimited.

17. DISTRIBUTION STATEMENT (of the abstract entered in Block 20, if different from Report)

18. SUPPLEMENTARY NOTES

19. KEY WORDS (Continue on reverse side if necessary and identify by block number)

20. ABSTRACT (Continue on reverse side if necessary and identify by block number)

The major environment Ultra Low Frequency (ULF), magnetic noise sources observed on the airborne AN/ASQ-81(V) optically pumped magnetometer are electromagnetic micropulsatrons, geological structures and ocean wave noise.

Experimental determinations of the amount of magnetic noise produced by ocean surface gravity waves were made. The author's current research designed to remove the wave noise and increase the probability of Magnetic Anomaly Detection (MAD) is summarized.

DD FORM 1 JAN 73 1473 EDITION OF 1 NOV 68 IS OBSOLETE
S/N 0102-014-6601 |
(Page 1)

SECURITY CLASSIFICATION OF THIS PAGE (When Data Entered)

Approved for public release; distribution unlimited.

Production of Ultra Low Frequency Magnetic Noise by Ocean Surface Gravity Waves and Its Real Time Removal from Airborne Magnetometer Measurements

by

James Francis Etro
Lieutenant, United States Navy
B.S. Oceanography, U.S. Naval Academy, 1973

Submitted in partial fulfillment of the
requirements for the degree of

MASTER OF SCIENCE IN METEOROLOGY AND OCEANOGRAPHY

from the

NAVAL POSTGRADUATE SCHOOL
December 1978

ABSTRACT

The major environmental Ultra Low Frequency (ULF), magnetic noise sources observed on the airborne AN/ASQ-81(V) optically pumped magnetometer are electromagnetic micropulsatrons, geological structures and ocean wave noise.

Experimental determinations of the amount of magnetic noise produced by ocean surface gravity waves were made. The author's current research designed to remove the wave noise and increase the probability of Magnetic Anomaly Detection (MAD) is summarized.

TABLE OF CONTENTS

LIST OF TABLES

LIST OF FIGURES

I. INTRODUCTION

Magnetometry has been used as a classical geophysical prospecting tool for years (Dobrin, 1952). The principles of magnetic anamoly analysis has also been applied to Anti-Submarine Warfare (ASW) with a limited amount of success for submarine localization.

The sensitivity of magnetometers has been continually improving so that it is now possible to observe, from an aircraft, fluctuatious of 10^{-2} nano Tesla/hertz (nT/Hz), imposed on the earth's constant field of approximately 50,000 nT.

Land stationed superconducting magnetic snesors have demonstrated a sensitivity of 10^{-6} nT/Hz. The advent of airborne superconducting magnetometers would greatly increase detection ranges; however, the extent of improvement depends in detail on the amplitude and frequency of the environmental noise which is above the noise floor of the instrument.

Airborne Magnetic Anomaly Detection (MAD) for ASW is done in the .04 to 2 Hz frequency band. Ocean surface gravity waves, in the .03 to 10 Hz frequency band (Silvester, 1974) are contributors to the magnetic noise spectrum. The other two major environmental noise sources are electromagnetic pulsations and geological noise.

It is generally assumed that noise due to ocean gravity waves is not "loud" enough to be of any consequence. However, experimentally it was observed that noise levels induced by

typical sea condition in the mid latitude oceans during the late fall to early spring are at least one order magnitude greater than the noise floor of airborne magnetometers. The noise greatly reduces the effectiveness of Magnetic Anomaly recognition.

II. THEORY

The problem of determining the electric current induced by deep water gravity waves at the ocean surface and the resultant periodic fluctuations in the magnetic field has been described by Weaver [1965]. The magnetic field fluctuations above and below the ocean were obtained by solving Maxwell's Equations for the magnetic flux density vector in air and water, and applying electromagnetic boundary conditions at the sea surface.

The movement of the sea surface through the earth's magnetic field induces electric eddy currents in the sea water. In deep water, assuming linear ocean wave theory, the water particle motion is periodic and circular, as is the induced magnetic field. This process becomes more complicated as one decomposes the sea surface spectrum into waves of various frequencies which may be propagating in various directions with respect to the magnetic field vector. Further complications arises as higher order wave theories are applied to describe the water particle motion and the waves propagate into shallow water.

A. MATHEMATICAL MODEL

The mathematical model of the induced field was developed by Weaver [1965], assuming linear wave theory to describe the water particle motion.

It was derived for a monochromatic ocean surface gravity wave, propagating in deep water, in the X direction. The development is summarized below.

The coordinate system formed a right hand triad as follows:

X-axis, was taken in the direction of wave propagation.

Y-axis, was taken parallel to the wave crest.

Z-axis, was taken downward into the sea, Z=0 at the still water level (SWL).

It was assumed that the earth's magnetic field was constant in the region, and the wave crest was infinitely long. The model became two dimensional as all magnetic gradients in Y were negligible.

The earth's vector magnetic field, $\vec{B}_e$, was expressed as

$$\vec{B}_e = |B_e|(\cos I \cos\Theta\,\hat{i} - \cos I \sin\Theta\,\hat{j} + \sin I\,\hat{k}),$$

where $\hat{i}$, $\hat{j}$, $\hat{k}$ were unit vectors along the three coordinate axis x, y, z. I, was the magnetic dip angle in the vertical plane, relative to the horizontal. Θ, was the inclination in the horizontal plane of the direction of wave propagation, clockwise from the magnetic meridian (see Figure 1).

The field vectors satisfied Maxwell's equation in the form

$$\nabla \times \vec{E} = -\frac{\partial \vec{B}}{\partial t}\,, \tag{1}$$

$$\nabla \times \frac{\vec{B}}{\mu_0} = \sigma\vec{E} + \sigma(\vec{v}\times(\vec{B}_e+\vec{B})) + \varepsilon\frac{\partial \vec{E}}{\partial t}\,, \tag{2}$$

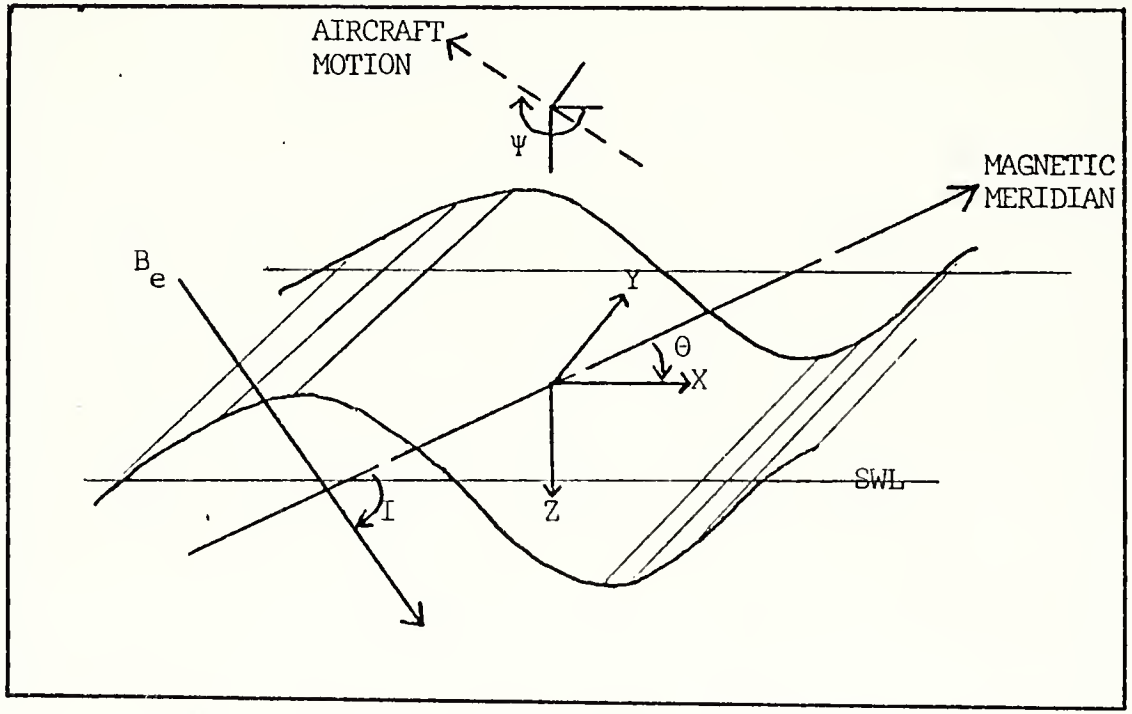

Figure 1. The model as it applies to a one component sea.

where $\vec{E}$ was the electric field vector ($^{\text{Volts}}/_{\text{Meter}}$), $\vec{B}$ was the induced magnetic flux density (Tesla), μ_o was the permeability of free space ($4\pi x10^{-7}$ $^{\text{Henry}}/_{\text{Meter}}$), σ was the electrical conductivity ($^{\text{Siemen}}/_{\text{Meter}}$), $\vec{V}$ was the water particle velocity vector ($^{\text{Meter}}/_{\text{sec}}$), ε was the permittivity ($^{\text{Farads}}/_{\text{Meter}}$), and t was time (seconds).

The deep water particle velocity, described by linear wave theory, was of the form

$$\vec{V} = a\omega(i\hat{i}+\hat{k})e^{i(\omega t - mx) - mz}, \tag{3}$$

where a was the wave amplitude (Meters), $\omega=2\pi/f$ was the angular frequency of the wave ($^{\text{Radians}}/_{\text{sec}}$), $m=2\pi/L$ was the wave number ($^{\text{Radians}}/_{\text{Meter}}$), and t was time (seconds).

Since $\vec{V}$ was harmonic in x and t, the magnetic and electrical field resulting from $\vec{V}$ has a similar structure, thus

$$\vec{B} = \vec{b}(z)\, e^{i(\omega t - mx)}, \tag{4}$$

$$\vec{E} = \vec{E}(z)\, e^{i(\omega t - mx)}. \tag{5}$$

The $\vec{B}$ field and the $\vec{E}$ field are non-divergent which implied

$$\frac{\partial b_z(z)}{\partial z} = i m b_x(z), \tag{6}$$

$$\frac{\partial E_z(z)}{\partial z} = i m E_x(z). \tag{7}$$

The differential equation in water satisfied by $\vec{B}$ was obtained by assuming $\vec{B} << \vec{B}_e$ and $\omega\varepsilon << \sigma$. Then, taking the curl of equation (2) and using the non-divergent portion of the vector identity, $\nabla \times (\nabla \times \vec{A}) = -\nabla^2 \vec{A} + \nabla(\nabla \cdot \vec{A})$, the following was obtained:

$$-\nabla^2 \vec{B} = \sigma \nabla \times \vec{E} + \sigma \mu_0 \nabla \times (\vec{V} \times \vec{B}_e) \quad . \tag{8}$$

Further simplification of equation (8) was obtained by the elimination of $\nabla \times \vec{E}$ by equation (1). From equation (3), $\vec{V}$ was eliminated. Then if $\gamma^2 = i\mu_o \omega \sigma$, the following equation results,

$$\frac{\partial^2 b(z)}{\partial z^2} = (\gamma^2 + m^2)\vec{b}(z) - \gamma^2 a_m (B_e(x) - iB_e(z))(i\hat{i} + \hat{k}) e^{-mz} \quad . \tag{9}$$

In region Z>0, equation (9) was solved for the Z component by assuming

$$b_z(z) = Q e^{-(\gamma^2 + m^2)^{1/2} z} + a_m (B_e(x) - iB_e(z)) e^{-mz} \quad ,$$

where Q was an undetermined coefficient.

In air $\varepsilon >> \sigma$, thus equation (2) became,

$$\nabla \times \frac{\vec{B}}{\mu_0} = \varepsilon \frac{\partial \vec{E}}{\partial t} \quad . \tag{10}$$

The curl of equation (10), when $\vec{E}$ was eliminated by equation (1), resulted in

$$\frac{\partial^2 \vec{b}(z)}{\partial z^2} = (m^2 - \mu_0 \varepsilon \omega^2)\vec{b}(z) \quad . \tag{11}$$

Confining the sea surface to scales of motion described by gravity waves implied that $m^2 >> \mu_o \varepsilon \omega^2$, thus

$$\frac{\partial^2 \vec{b}(z)}{\partial z^2} = m^2 \vec{b}(z) \quad . \tag{12}$$

In the region Z<0 the solution for the Z component of equation (12) was of the form

$$b_z(z) = R e^{mz} \tag{13}$$

where R was an undetermined coefficient.

The magnetic field vector was continuous across the air-sea interface, thus, the following boundary condition at Z=0, existed:

$$b_{z\,AIR}(z=0) = b_{z\,WATER}(z=0) \tag{14.a}$$

$$\frac{\partial b_{z\,AIR}(z=0)}{\partial z} = \frac{\partial b_{z\,WATER}(z=0)}{\partial z} \tag{14.b}$$

Applying the above boundary values to equations (9) and (13) yielded

$$R = Q + a\,m\,(B_e(x) - i\,B_e(z)) \quad , \tag{15}$$

and

$$mR = -Q(\gamma^2 + m^2)^{1/2} - a\,m^2\,(B_e(x) - i\,B_e(z)) \quad . \tag{16}$$

Equations (15) and (16) lead to

$$Q = \frac{-2m^2 a\,(B_e(x) - i\,B_e(z))}{m + (\gamma^2 + m^2)^{1/2}} \tag{17}$$

and

$$R = \frac{a_m \left(B_x(x) - i B_z(z)\right)\left((\gamma^2 + m^2)^{1/2} - m\right)^2}{\gamma^2} \quad . \qquad (18)$$

Thus the Z component of the induced magnetic field vector in air was

$$b_z(z) = \frac{a_m \left(B_x(x) - i B_z(z)\right)\left((\gamma^2 + m^2)^{1/2} - m\right)^2 e^{mz}}{\gamma^2} \quad . \qquad (19)$$

In order to further simplify equation (19), $\frac{\gamma^2}{m^2} << 1$ was true for gravity waves resulting in

$$b_z(z) = \frac{a\gamma^2}{4m} \left(B_x(x) - i B_z(z)\right) e^{mz} \quad . \qquad (20)$$

From equation (6) and (20) it was seen that

$$i b_x(z) = b_z(z) \qquad (21)$$

It was convenient to measure the earth's field with a total field magnetometer. Thus,

$$B_{MEASURED} = B_e + b_x(z) \cos I \cos\theta + b_z(z) \sin I \quad . \qquad (22)$$

When equations (20) and (21) were used to simplify equation (22), and only the perturbations were considered, it can be shown that the magnitude of the observed magnetic field at a specific frequency would be,

$$b(f) = \frac{a\sigma\mu_0\omega}{4m} \left|\vec{B}_e\right| \left(\left(\cos I \cos\theta\right)^2 + \left(\sin I\right)^2\right) e^{mz} \quad , \qquad (23)$$

$$z < 0 \quad .$$

The deep water wave length (L) of a surface wave is related to the wave period (T) by,

$$L = \frac{gT^2}{2\pi} \tag{24}$$

where g is the acceleration due to gravity.

Eliminating m, from equation (23) by the use of equation (24) leads to,

$$b(f) = \frac{a\sigma\mu_0 T g}{8\pi} |\vec{B}_e| \left((\cos I \cos\theta)^2 + (\sin I)^2\right) e^{\frac{4\pi^2}{gT^2} z} \tag{25}$$

Equation (25) was used to model the magnetic field spectrum when the directional ocean wave spectrum was known.

Using an airborne magnetometer to measure the magnetic spectra, there was a doppler type frequency shift, described as,

$$f' = f(1 - (2\pi f u/g)\cos\psi) \tag{26}$$

(see Appendix C). Where f' was the wave frequency observed on the aircraft (sec^{-1}), f was the actual wave frequency, u was the velocity of the aircraft ($^{Meter}/sec$), and ψ was the angle between aircraft motion and direction of wave propagation (see Figure 1).

III. THE EXPERIMENT

Magnetic data was collected by an airborne magnetometer flown over the sea surface in order to verify the theory previously presented and to further understand the observed environment in the 0 to 2Hz band. The AN/ASQ-81 magnetometer, aboard the P-3C Orion aircraft, is capable of measuring the signal produced by ocean gravity waves which are frequency shifted due to relative motion between the wave and the aircraft flying at 100 meters altitude. The analog voltage time series output of the magnetometer was recorded on an HP3960, FM tape recorder for post flight analysis.

The fluctuation of the sea surface below the aircraft was determined by two techniques. The analog voltage time series output of the APN-194 radar altimeter, also aboard the aircraft, was recorded.

Independent of the aircraft data the ocean surface wave climate was determined from analysis of the Fleet Numerical Weather Central (FNWC), spectral Ocean Wave Model (SOWM) and measured wave spectrum from National Oceanic and Atmospheric Administration (NOAA), Environmental Buoy, NR-6003 (EB-17), located at 52.2N, 155.8W from the airborne data.

The airborne data was collected in vicinity of 52°N, 156°W, around the buoys' reporting period, 00Z, 10 Feb 78.

A. AIRBORNE DATA COLLECTION

The AN/ASQ-81 employs the atomic properties of optically pumped, metastable helium atoms to detect variations in total

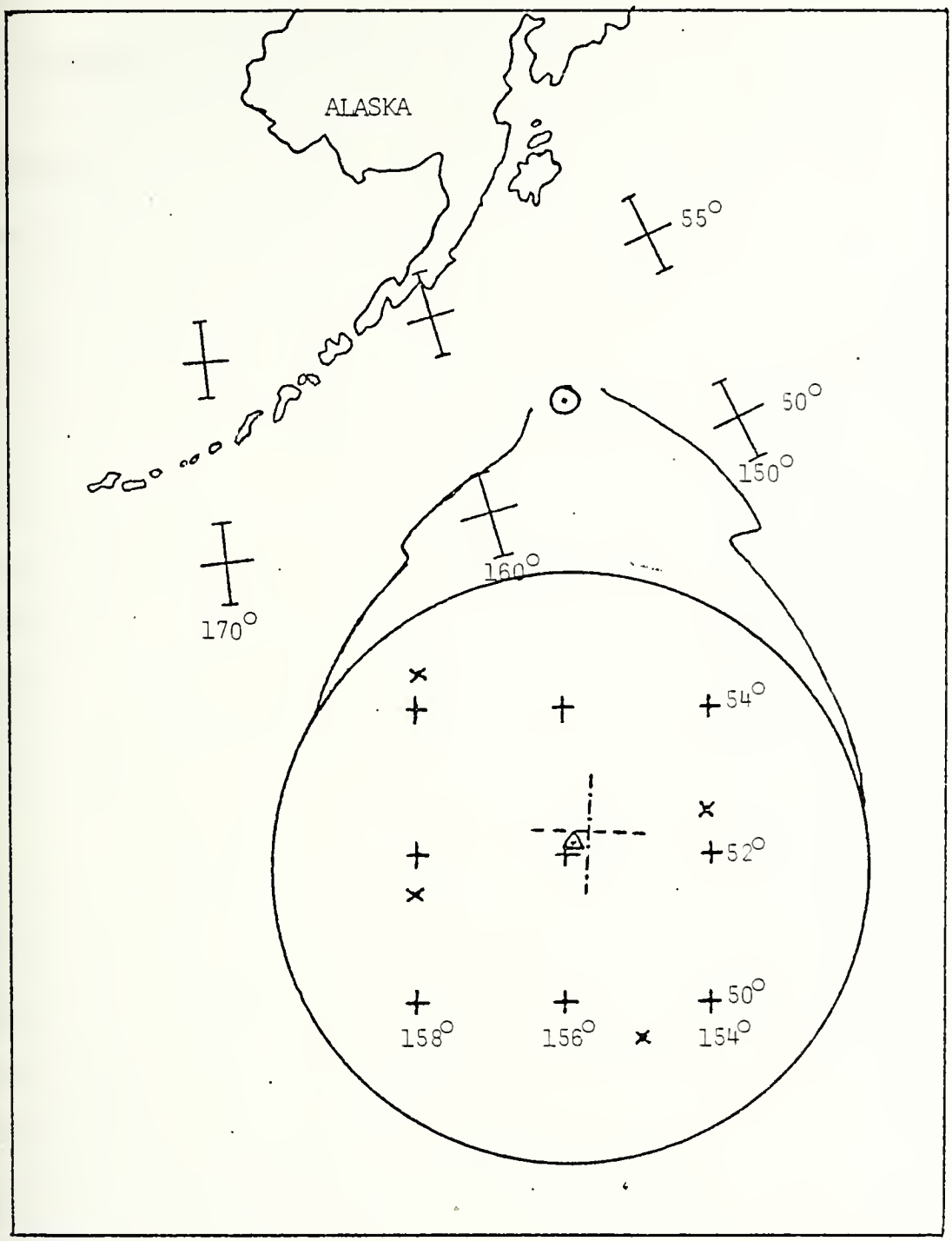

Figure 2. Region of data collection. (X) FNWC Grid Points, (Δ)NOAA Buoy, (---) First Leg of Aircraft Data, (-.-.) Second Leg of Aircraft Data.

field magnetic amplitudes. The output of the sensing element is converted to an analog voltage which is bandpassed and scaled to display field variations (Order 10^{-11}T) as a function of time. Instrument specifications are described in Appendix A.

Perpendicular legs, 270° True and 000° True, were flown at approximately 60 meters altitude and 180 knots (91.44 M/s) for 30 minutes each. (See Figure 2) The magnetic data was collected in the .04 Hz to 2 Hz band, thus, eliminating the earth's constant field and any micropulsations above 2 Hz. Aircraft motions were compensated for by the magnetometer using baroaltimetry, selective filtering and accelerometers. No variations in the magnetic field due to the aircraft were expected due to the above real time processing and the straight and level flight paths flown.

The instantaneous aircraft altitudes were recorded simultaneously with the magnetic data from the APN-194 radar altimeter, which responded linearly to apparent altitude changes due to long period surface gravity waves. The wave frequency was shifted due to aircraft motion (see equation (26)). Beam characteristics, 60° cone, were such that at 60 meters the diameter of the radar spot on the surface was approximately 70 meters. In order to resolve wave amplitudes from 60 meter altitude, the wave period must be greater than 10 seconds. The frequency and amplitude errors attributable to the size of the radar spot were considered in the analysis.

The AN/ASQ-81 and APN-194 signal pick-off points are described in Appendix A.

B. SPECTRAL WAVE DATA COLLECTION

The experiment was conducted around synoptic reporting period 00Z, 10 Feb 1978 in vicinity of NOAA Buoy, EB-17, so the spectral information computed by the Buoy for the 00Z time period was useful in interpreting the aircraft data.

In addition to Buoy data the SOWM output was used in order to infer directionality and improve the spectral wave estimate in the region of the flight.

The Buoy is designed to report meterological and oceanographic conditions at the sea surface every 3 hours. The wave conditions are measured for 20 minutes by accelerometers and reported for the Buoy location as frequency and amplitude (Steele and Johnson, 1977). The Buoy data of 00Z, 10 Feb 1978 is reported in Table I.

Frequency (Hz)	Period (sec)	Amplitude (meters)
.06	16.7	.8322
.07	14.3	.7574
.08	12.5	1.6064
.09	11.1	1.9604
.1	10.0	1.9312
.11	9.1	1.5419
.12	8.3	1.0116
.13	7.7	.9083
.14	7.1	.7917
.15	6.7	.6543
.16	6.3	.4793
.17	5.9	.4511
.18	5.6	.4212

Table I
NOAA Data Buoy 00Z, 10 Feb 1978

The FNWC, SOWM uses the analyzed surface pressure field to determine wind velocities and then builds, radiates and dissipates waves as prescribed by wave theory (FNWC Tech Note No. 75-3). Model output is energy as a function of frequency and direction at each grid point. The wave energy (E) at a frequency can be converted to wave amplitude (a) by $a = E \cdot \Delta f$.

SOWM frid coverage of the data area is shown in Figure 2. The model output for the closest grid point is summarized in Table II.

DIRECTION FROM (^{o}T)	283^{o}	313^{o}	343^{o}	013^{o}
PERIOD (SEC)		AMPLITUDES (METERS)		
16.4	.347	0	.578	.347
14.93	.578	.408	1.002	.578
13.89	.708	1.293	1.082	.347
12.82	1.636	0	1.686	1.686
12.04	1.227	1.686	1.157	.959
10.99	1.417	1.584	.914	1.192
9.71	1.293	1.493	.944	1.436
8.5	.944	1.356	1.227	1.271
7.5	.851	.973	.987	.914
6.5	.409	.457	.354	.167

Table II

FNWC, SOWM Data, 03Z 10Feb78. Grid point located at 52.357N, 154.099W. Amplitudes (meters)

IV. DATA ANALYSIS

A. TIME SERIES ANALYSIS

The general form of the magnetic and altitude time series is shown in Figure 3, which is a sample of each time series.

The time series were digitized at .1 second intervals, resulting in a Nyquist frequency of 5 Hz. Any spectral power above 5 Hz would be folded back into the spectral estimate (alliasing). The magnetic data, due to the low pass, 2 Hz, characteristics of the instrument, alliased only instrument noise which was at a low level. It was assumed that no significant alliasing of the altitude data occurred due to the altimeters 0.1 second RC constant which results in a 1.59 Hz cutoff frequency ($\omega_c = {}^{1}/RC$).

Prior to computing power spectral estimates, the data was calibrated to insure constancy of unit magnitudes. The magnetic data voltages were linearly calibrated to nT and the altimetry voltages were linearly calibrated to meters after the flight.

The data was prepared for the Fast Fourier Transform (FFT), (Bendat and Piersol, 1971) by forming 16 ensembles, 102.4 seconds each. Each ensemble was then linearly detrended. The detrending removed significant variance from the frequencies below .001 Hz. The cosine function was used to taper 10% of the time series by multiplying the first and last 51 points of the time series by the cosine. Points 1 and 1024 become zero and points 52 thru 973 are as digitized. The tapering procedure is done in order to prevent non-real low frequency power leakage, due to

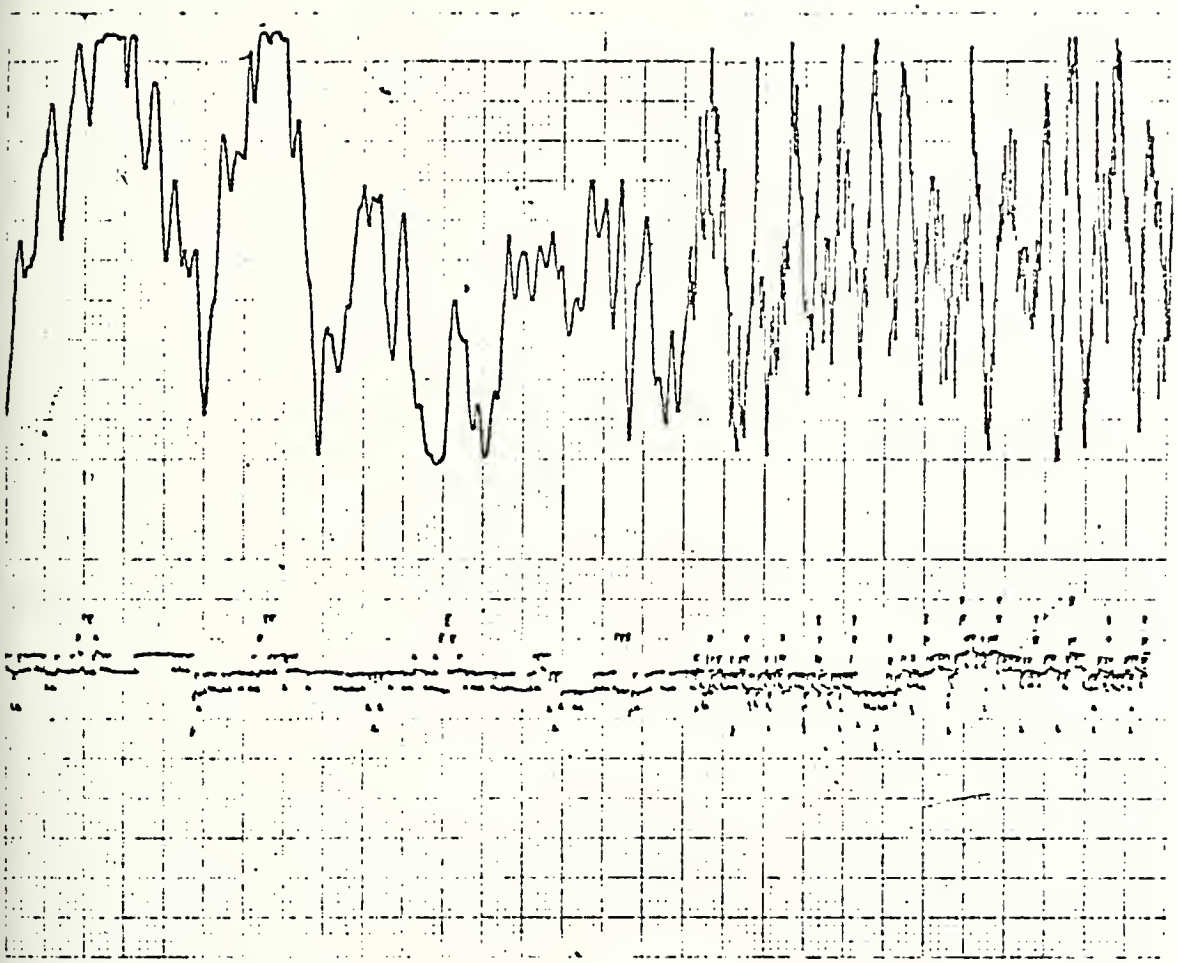

Figure 3. Sample of magnetic time series (top) and altitude time series (bottom). Horizontal scale is 1mm/sec. Vertical scale is 1mm/volt.

ensemble averaging, into the spectrum. The variance removed in the time series taper is restored to the power spectra after the FFT (Bendat and Piersol, 1971).

The FFT computes the real and imaginary components of the Fourier Transform. It was then possible to compute the sample power spectra of each signal by ensemble averaging. The normalized cross power spectra, defined as coherence and the phase of the cross power spectrum between signals were also computed.

Each of the two flight courses were treated as separate data sets. Note in Figure 4 the power spectra of the altimeter (M^2/Hz) and magnetometer (nT^2/Hz) and the coherence and phase as a function of frequency. The numerical results are summarized in Appendix D.

B. SPECTRAL WAVE ANALYSIS

The analysis of the FNWC, SOWM directional wave spectra and EB-17 ocean wave amplitude spectra in order to describe the magnetic field variations observed aboard the aircraft, required fitting the large scale information to the microscale. This change of scale was feasible due to spatial uniformity of the ocean wave spectra over the area and frequency range investigated.

The ocean wave climate in an area can be described by that at a point over a period of time. EB-17 reported the waves during a 20 minute period to have the spectral shape listed in Table I. The FNWC ocean wave amplitude and directional spectra had a similar shape listed in Table II.

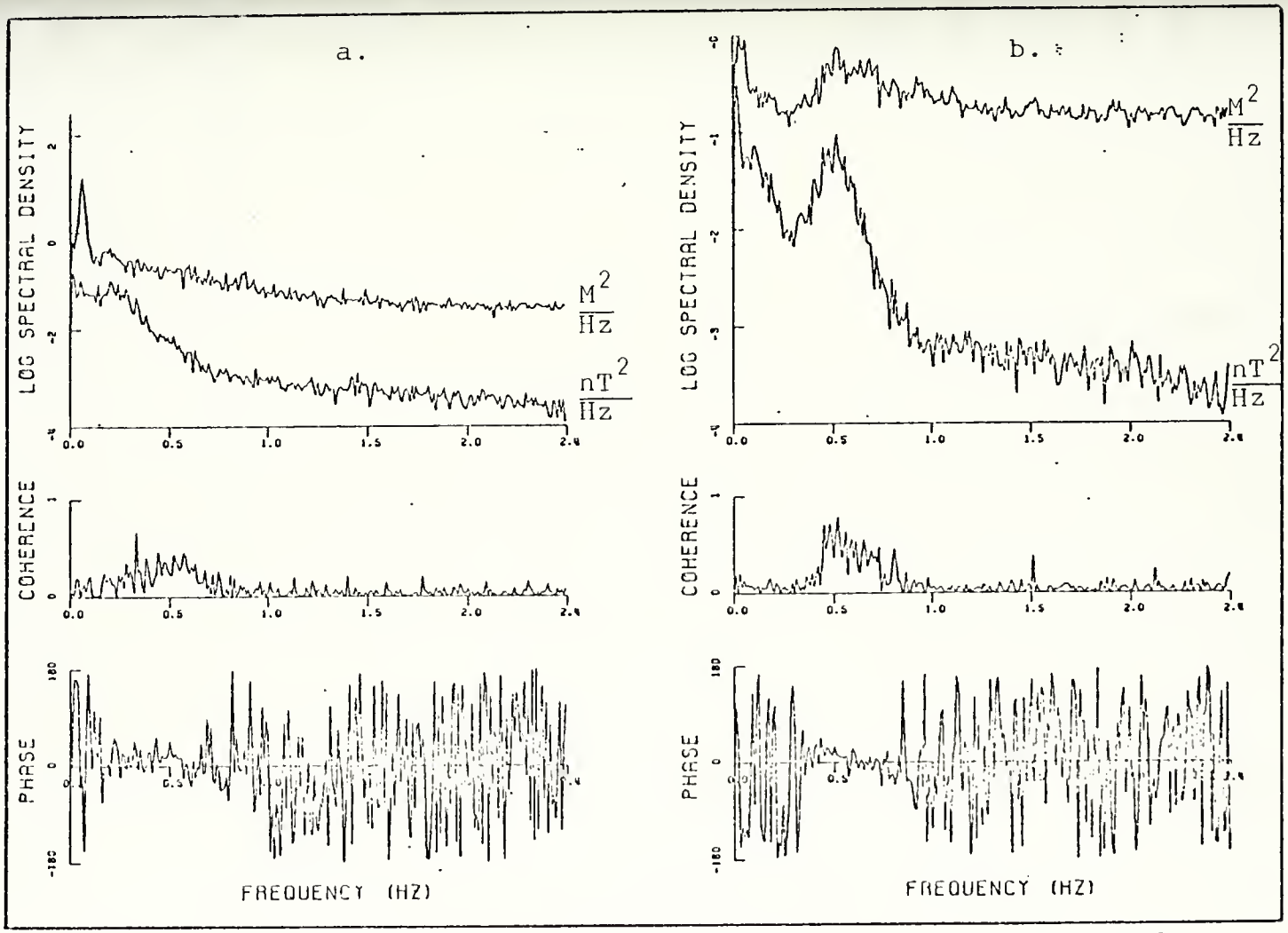

Figure 4. Altitude power spectrum ($\frac{M^2}{Hz}$), magnetic power spectrum ($\frac{nT^2}{Hz}$), coherence and phase functions. 32 degrees of freedom. Nyquist frequency is 5 Hz. 4a, aircraft course 270°T, 180 knots, 60 meters altitude. 4b, aircraft course 000°T, 180 knots, 60 meters altitude.

The directionality of wave components at EB-17 was determined by group velocity analysis (Silvester, 1974) which propagated the FNWC, SOWM data at nearby grid points to the buoy position. The greatest weight was on the grid point closest to the position of the buoy. The grid point was located at 52.357N, 154.099W, 60 miles from the buoy. The analyzed buoy directional amplitude spectra is reported in Table III.

PERIOD (SEC)	AMPLITUDE (METERS)	DIRECTION FROM (°T)
16.7	.8322	340°
14.3	.7574	340°
12.5	1.6064	315°
11.1	1.9604	315°
10.0	1.9312	320°
9.1	1.5419	320°
8.3	1.0116	320°
7.7	.9083	320°
7.1	.7917	330°
6.7	.6543	330°
6.3	.4793	320°
5.9	.4511	320°
5.6	.4212	320°

Table III
Analyzed directional wave data at NOAA buoy EB-17, 00Z 10 Feb 78.

It is important to note that the NOAA data and the FNWC data have similar spectral shapes although amplitudes are not equal, verifying scale analysis assumptions. The buoy reports a spectral peak at approximately 11 seconds. FNWC predicts a spectral peak at approximately 12 seconds.

The observed ocean wave climate on the aircraft, although similar, was not the climate observed by EB-17 or predicted by SOWM. Each of the ocean wave data sources had errors associated with them, which would contribute to the differences in the data. Scale considerations, length of airborne data record, modeled grid point locations, buoy location and flight path, further contribute to the uniqueness of the separate data sources.

Due to the multidirectional nature of the SOWM data and its proximity to the flight path, it was assumed that the closest FNWC data point (Table II) most closely resembled the ocean wave climate observed on the aircraft. The SOWM wave information was applied to equation (25) resulting in an expected magnetic amplitude spectrum. The expected frequency shift due to the aircrafts motion relative to the waves was computed by applying equation (26). To be consistent with the power spectral density computed from the aircraft data the amplitude spectrum described above was squared and normalized by multiplying by the frequency interval of each frequency estimate. The results are summarized in Figure 5 and numerically in Appendix D.

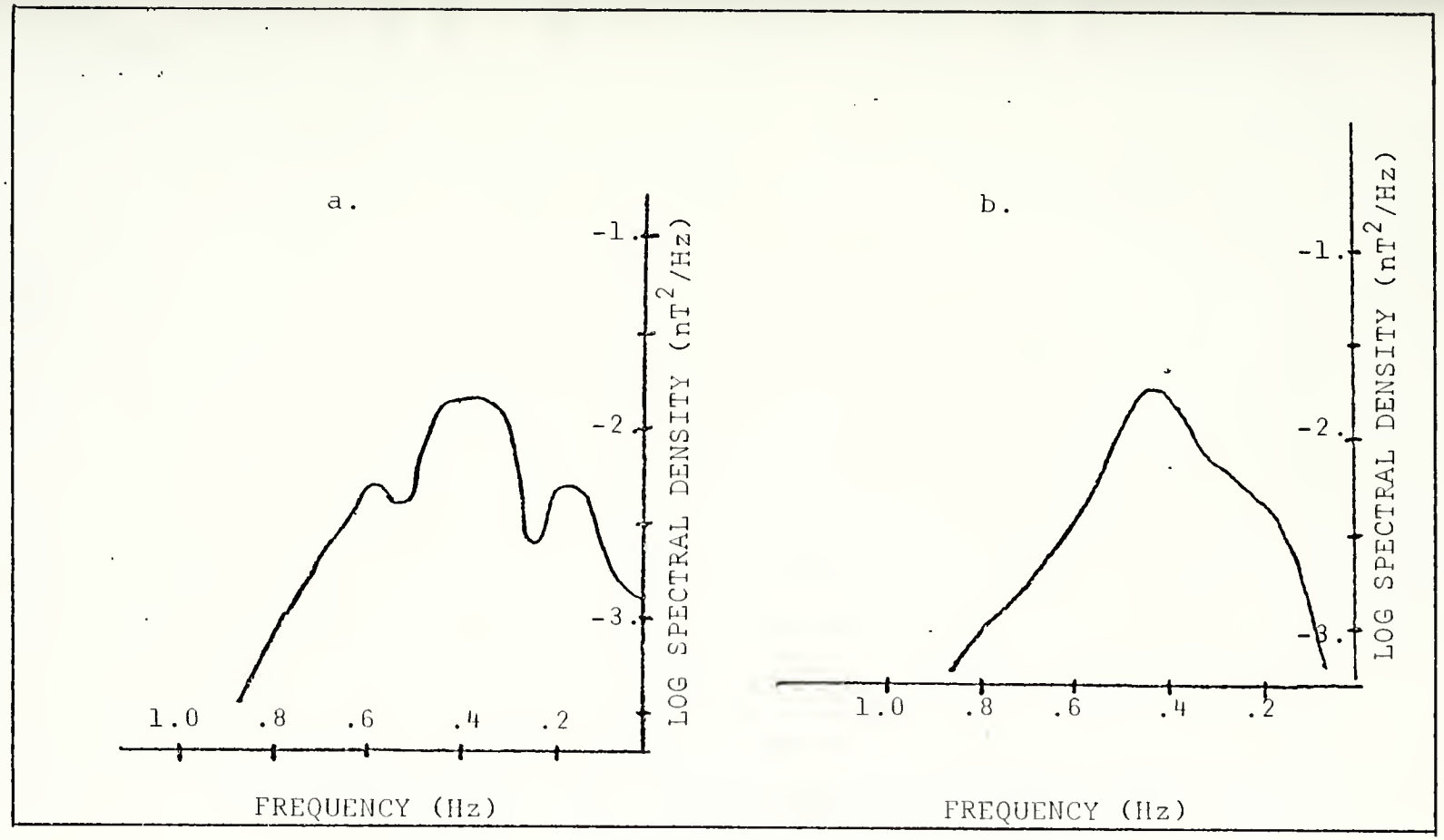

Figure 5. Magnetic spectra computed from SOWM data applied to equations 25 and 26.
5a, data generated for 270° aircraft motion.
5b, data generated for 000° aircraft motion.

V. DISCUSSION

Baker and Graefe (1968) showed experimentally that the theory reviewed in Section II describes the magnetic field induced by ocean surface gravity waves. Comparison of the aircraft magnetic power spectra, Figure 4, and the expected magnetic power spectra computed from SOWM data, Figure 5, further verifies the electromagnetic theory described above.

Figure 6, which is the superpositioning of Figure 4a on Figure 5a and Figure 4b on Figure 5b, illustrates that although the aircraft and wave data magnetic spectra are not the same they are similar in amplitude and frequency. The differences observed in the low frequency end can, in part, be attributed to the assumptions necessary to the formulation of each magnetic power spectrum and the assumption that each data source is stationary in time and space.

The FNWC data, although close to the flight path, was not coincident with the aircraft track (see Figure 2). Furthermore, determining the barometeric surface pressure field over data sparse areas, such as the Gulf of Alaska caused inaccuracies in the SOWM wave height, frequency and directional information, which could have contributed to some of the differences observed.

When studying the magnetic spectrum computed from the aircraft data it cannot be assumed that the only source of noise was the ocean gravity waves. Although no significant electromagnetic micropulsations in the 0 to 2 Hz frequency band, were expected, they cannot be ignored.

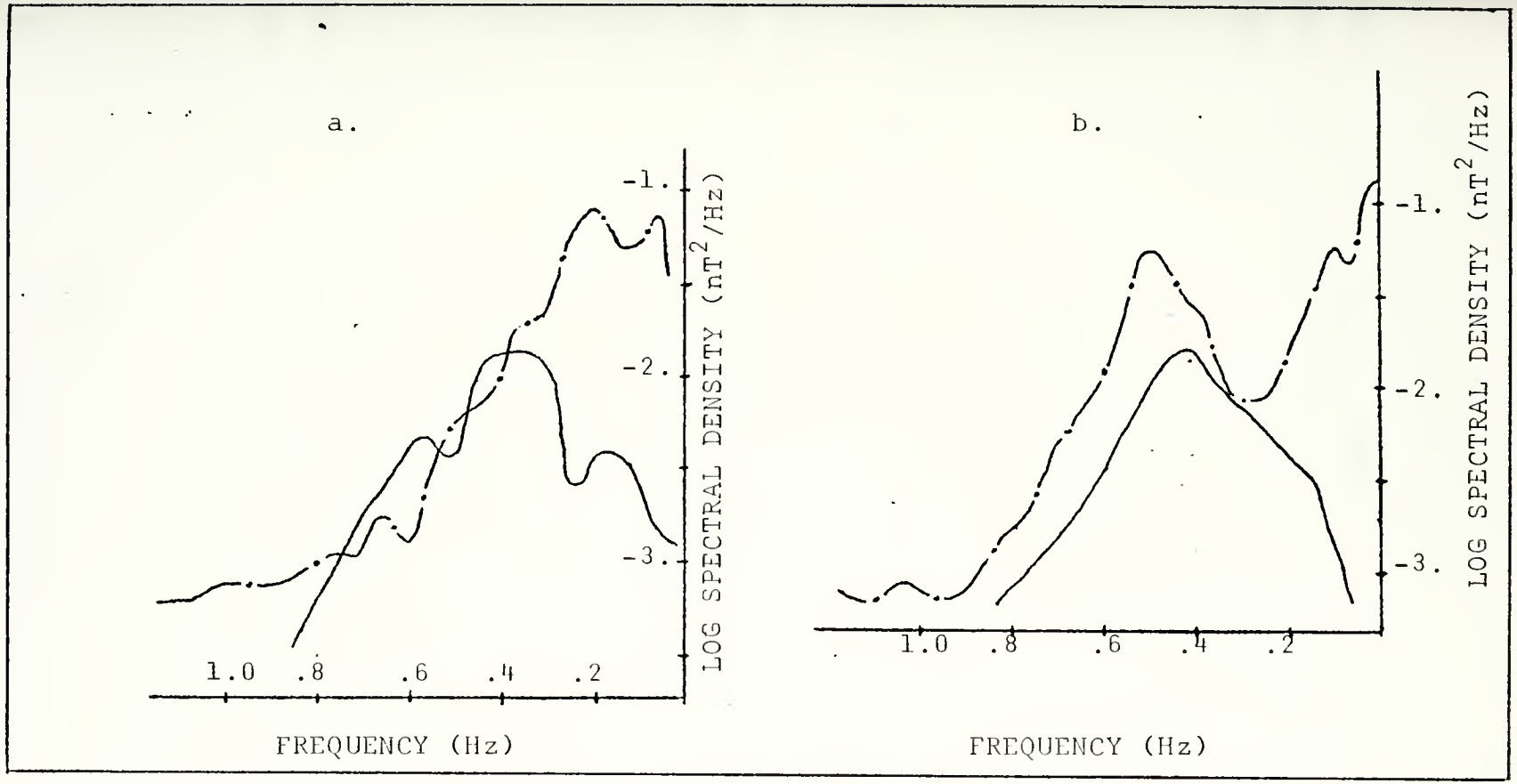

Figure 6. Superposition of magnetic spectra observed from aircraft (——·—) and magnetic spectra computed from SOWM data applied to equations 25 and 26.
6a is data from first leg of aircraft flight.
6b is data from second leg of aircraft flight.

Production of magnetic noise by the aircraft's motion and onboard equipage was considered. Ideally, most aircraft produced noises were compensated for in the magnetometers real time processing scheme and the flight was straight and level on each leg which would further reduce noise. However, experience shows that the noise sources described above are not completely removed from the spectral analysis when long data records are required.

Note in Figure 6a that both the aircraft and the analyzed SOWM magnetic power spectra indicate a broad coincident frequency band. In Figure 6b it is seen that a change in the flight path causes the band width of coincidence to compress, shift to higher frequency, and two distinct maxima are observed in the aircraft spectrum. One of which is nearly coincident with the SOWM magnetic spectrum. This indicates that a significant magnetic noise source is external to the aircraft and ocean surface wave dependent.

Most significant, is the information implied from the analysis of Figure 4 and Figure 6. It is seen (Figure 4) that the coherence is high and the phase relationship is good between the magnetometer and the altimeter in a small frequency band (.2 to .7 Hz). The trend observed in the phase relationship over that band can be attributed to signal delays imposed by the electrical characteristics of each instrument.

This highly correlated frequency band falls in the same band in which the ocean gravity wave noise is expected. The

altimeter specifications indicated that it was accurate, ± 1 foot and has a linear response to about 1.5 Hz. Thus it can be concluded that the altimeter senses the sea surface flucuations.

Note the large spectral peak below .1 Hertz on the altimeter power spectra of Figure 4. The peak is approximately one order of magnitude greater in the data of the first flight leg (Figure 4a) when compared to the second (Figure 4b). This peak was due to an intermittent square wave caused by malfunction of the altimeter. The square wave does not significantly degrade the analysis presented above.

VI. APPLICATION

It was shown in section V that the altimeter can be used to describe the instantaneous fluctuations of the sea surface below the aircraft which are directly related to a portion of the magnetic noise. Thus, the high correlation between the altimeter and the magnetometer indicates that it is possible to remove a portion of the magnetic noise due to ocean surface gravity waves.

Current Naval ASW tactics require that the magnetic field information be analyzed in the real time domain. Thus, noise cancelling must be done real time.

Spectral analysis or convolution filtering is not practical due to the signal characteristics of the target anomaly and the long length of records required to compute the FFT which describes the low frequency signals.

The magnetic anomaly is a single transient signal imposed on the total magnetic field thus making spectral analysis impossible. Furthermore, it is possible that the aircraft may change direction and flight attitude before a sufficiently long record is collected from the altimeter and the magnetometer to determine the coefficients of the Fourier Transform for convolution filtering.

In order to keep noise removal in the real time domain the principle of Adaptive Noise Cancelling (Widrow, et.al., 1975) was applied to the 10 Feb. data.

The adaptive noise cancelling was done by a microprocessor developed at Naval Oceans System Center (NOSC) and already used in frequency analysis at frequencies higher than those analyzed for ultra low frequency magnetic information (0-2 Hz). The altimeter (reference signal) contained noise that was correlated with noise in the magnetometer (primary signal). Each signal was digitized and the algorithm used computed the solution which removed the correlated noise from the primary by adaptively subtracting the reference signal to converge on minimum power in the primary signal.

Preliminary results indicate that this method may be useful for real time noise cancelling in airborne magnetic data (see Figure 7 and Figure 8) while the magnetic anomalies not due to wave motion should be relatively unaffected.

Note in Figure 7 the relative signal levels before and after noise cancelling. The signal appears to be cut in gain approximately four to one after noise cancelling. However, spectral analysis (Figure 8) indicates that the only power reduction was in the frequency band that has been indentified as the ocean surface gravity wave noise frequency band.

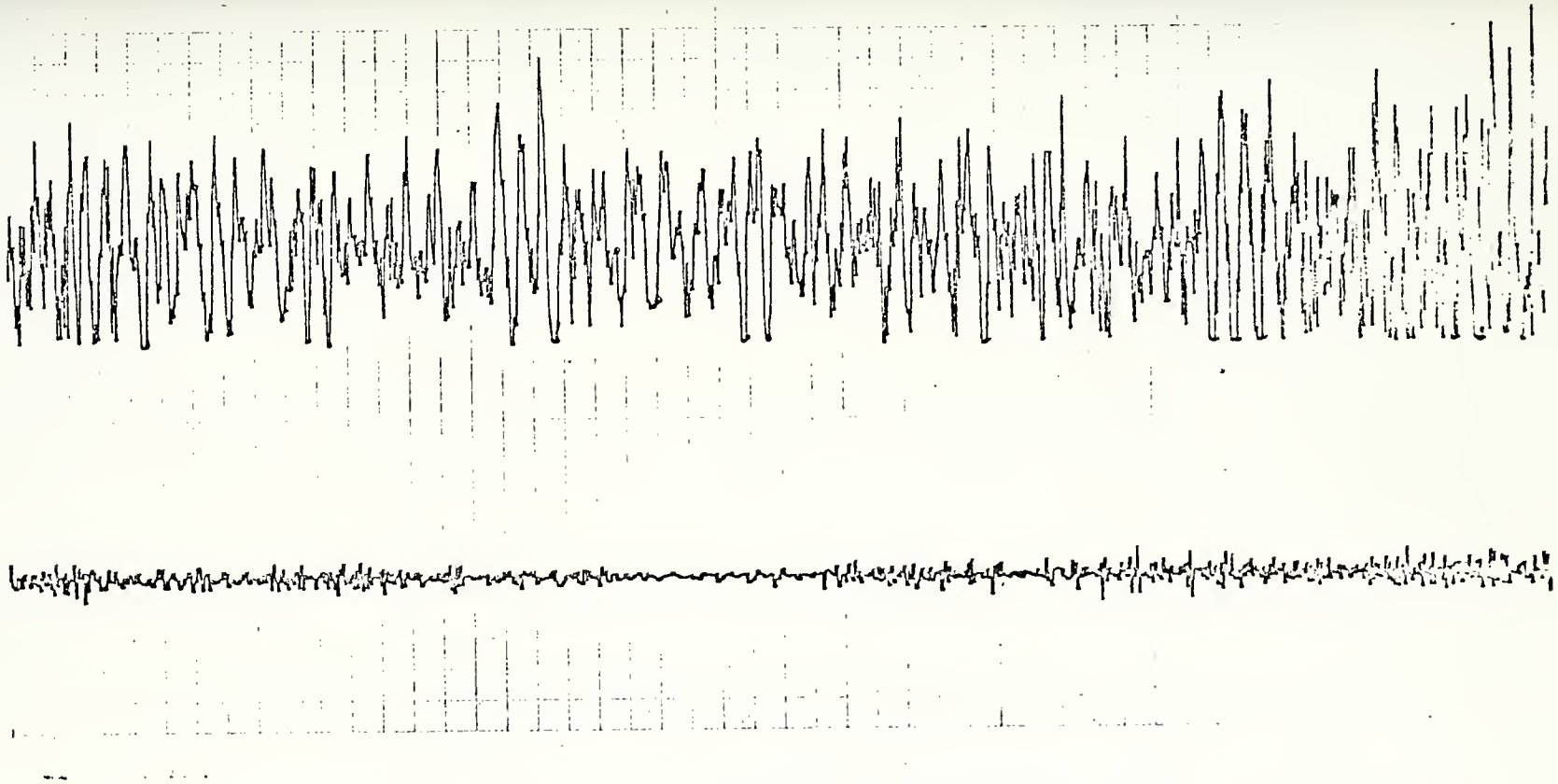

Figure 7. Magnetic time series (top). Wave noise cancelled time series (bottom). Horizontal scale is 1mm/sec. Vertical scale is 1mm/volt.

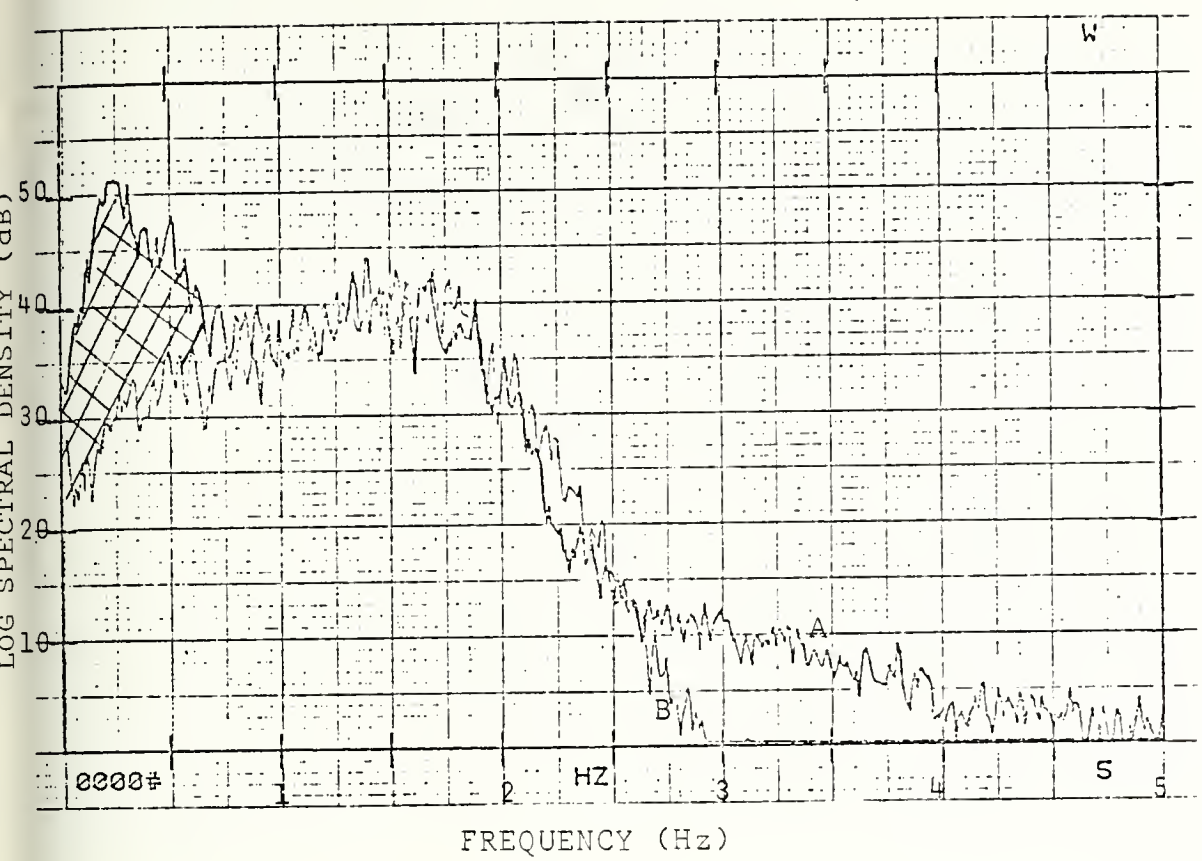

Figure 8. Aircraft magnetic spectrum (A) compared to "noise cancelled" magnetic spectrum (B). When altimeter was used as noise reference. Each spectrum has 16 degrees of freedom. Note the band limited noise reduction indicated by the cross hatched area.

VII. SUMMARY

It has been shown that ocean surface gravity waves contribute significantly to the environmental background noise observed in airborne magnetometry. The noise is the result of the magnetic field associated with electrical eddy currents induced by ocean wave propagation through the earth's magnetic field.

The APN-194 altimeter aboard the P-3C ORION aircraft is capable of describing the wave climate below the aircraft simultaneously with total field magnetic measurements observed by the AN/ASQ-81(V) magnetometer, also aboard the P-3C. Thus, the altimeter can be used to infer the wave noise measured by the magnetometer.

Analysis demonstrated that it is possible to remove a significant portion of the magnetic noise due to ocean gravity waves by using the altimeter as a noise reference and subtracting that processed reference in real time from the magnetometer time series output.

Further research with real submarine targets is underway in order that the ASW community will benefit from applications of this work. Development of a greatly improved magnetometry system is possible in the near future.

APPENDIX A
MAGNETOMETER AND ALTIMETER SYSTEM CHARACTERISTICS

I. MAGNETOMETER SYSTEM PARAMETERS - AN/ASW-81(V) MAGNETOMETER GENERAL CHARACTERISTICS

Performance-Magnetometer Group

Range	23,000 to 75,000 gammas
Noise level	0.016 gamma (peak-to-peak)
Figure of merit (FOM)	0.24 gamma
MAD bandpass (selectable)	
High Pass	Corner frequencies 0.04, 0.06, 0.08, and 0.1 Hz Rejection slope 36 dB/octave
Low Pass	Corner frequencies 0.2, 0.4, 0.6, and 2.0 Hz Rejection slope 24 dB/octave
Gain selection (full scale)	0.1, 0.2, 0.4, 1, 2, 4, 10, 20, and 40 gammas
Altitude compensation	Barometric type Reference altitude, self-zeroing Linear range, $\pm$ 200 feet

Environmental Limits

This equipment meets the requirements of military specification MIL-E-5400 within the limits described below.

Temperature

(1) Equipment Operating: -54°C to 71°C except the Magnetic Detector DT-323/ASQ-81(V) or Towed Body TB-623/ASQ-81(V) which have +55°C maximum temperature.

(2) Equipment Nonoperating: -62°C to +85°C except the Magnetic Detector DT-323/ASQ-81(V) or Towed Body TB-623/ASQ-81(V) which have +71°C maximum temperature.

Altitude	Sea level to 30,000 feet
Humidity	0 to 100 percent

Shock	Up to 15 g with duration of 11 ±1 milliseconds
Vibration	Curve IV (10 g, 5 to 500 Hz) except Detecting Set Control C-6983/ASQ-81(V) or C-9086/ASQ-81(V) which are curve III (5 g, 5 to 500 Hz).

Input Power Requirements

Magnetometer Group

115/200 volts ac 3-phase power

Voltage limits	108 to 118 volts
Frequency limits	380 to 420 Hz
Power	150 VA maximum

Panel Lamp Power

Voltage limit	0 to 28.5 volts
Frequency	dc or ac
Power	10 watts maximum

Mangetometer Pick off Points

Signal pick off points in the P-3C were Rack C-3, TB-433, pins C-14 and C-15.

II. ALTIMETER SYSTEM PARAMETERS -
AN/APN-194 RADAR ALTIMETER

Manufactured by Honeywell, Inc., Government and Ared Products Division

Specifications

±1 ft. accuracy to 40,000 ft

60° beam width to 3dB point

.1 sec RC constant

25-35 nano second pulse

0-25 nsec gate

Altimeter Pick off Points

Signal pick off in the P-3C were FS 1005, TB-416, pins A-5 and A-6.

Table B-1 NOAA Buoy (6003), EB-17 Reported Data for 21Z 9 Feb 1978, 00Z 10 Feb 1978 and 03Z 10 Feb 1978.

BUOY: 6003 DATE ACQUIRED: 2-10-78 02

SEA DISP.	SPEC. PERIOD	LOW FREQ. WAVE HT.	LOW FREQ. WAVE PD.	HIGH FREQ. WAVE HT.	HIGH FREQ. WAVE PD.
0.0000E	0100.0	0.0	0.0	4.3	8.7
0.0000E	0 50.0	0.0	0.0	4.3	8.7
0.0000E	0 33.3	0.0	0.0	4.3	8.7
0.0000E	0 25.0	0.0	0.0	4.3	8.7
0.6094E	-1 20.0	0.0	20.0	4.3	8.7
0.4329E	1 16.7	0.6	16.7	4.3	8.7
0.3585E	1 14.3	1.0	15.9	4.2	8.6
0.1813E	2 12.5	1.6	13.7	4.2	8.5
0.2402E	2 11.1	2.4	12.4	4.0	8.3
0.2331E	2 10.0	3.1	11.6	3.5	7.8
0.1486E	2 9.1	3.6	11.0	3.0	7.1
0.6397E	1 8.3	3.8	10.6	2.4	6.4
0.5157E	1 7.7	3.9	10.4	2.0	5.8
0.3917E	1 7.1	4.0	10.2	1.7	5.5
0.2676E	1 6.7	4.1	10.0	1.5	5.1
0.1436E	1 6.3	4.1	9.9	1.3	4.8
0.1272E	1 5.9	4.1	9.8	1.2	4.6
0.1109E	1 5.6	4.2	9.7	1.1	4.4
0.9849E	0 5.3	4.2	9.6	1.0	4.3
0.7812E	0 5.0	4.2	9.5	1.0	4.1
0.6923E	0 4.8	4.2	9.4	0.9	4.0
0.6033E	0 4.5	4.2	9.3	0.8	3.9
0.5143E	0 4.3	4.2	9.2	0.7	3.8
0.4254E	0 4.2	4.2	9.2	0.7	3.7
0.3811E	0 4.0	4.2	9.1	0.6	3.6
0.3370E	0 3.8	4.2	9.0	0.6	3.5
0.2929E	0 3.7	4.3	9.0	0.5	3.4
0.2487E	0 3.6	4.3	8.9	0.5	3.3
0.2273E	0 3.4	4.3	8.9	0.4	3.3
0.2059E	0 3.3	4.3	8.8	0.4	3.2
0.1845E	0 3.2	4.3	8.8	0.3	3.2
0.1631E	0 3.1	4.3	8.7	0.3	3.1
0.1417E	0 3.0	4.3	8.7	0.2	3.1
0.0000E	0 2.9	4.3	8.7	0.1	3.0
0.0000E	0 2.9	4.3	8.7	0.0	0.0
0.0000E	0 2.8	4.3	8.7	0.0	0.0
0.0000E	0 2.7	4.3	8.7	0.0	0.0
0.0000E	0 2.6	4.3	8.7	0.0	0.0
0.0000E	0 2.6	4.3	8.7	0.0	0.0
0.0000E	0 2.5	4.3	8.7	0.0	0.0
0.0000E	0 2.4	4.3	8.7	0.0	0.0
0.0000E	0 2.4	4.3	8.7	0.0	0.0
0.0000E	0 2.3	4.3	8.7	0.0	0.0
0.0000E	0 2.3	4.3	8.7	0.0	0.0
0.0000E	0 2.2	4.3	8.7	0.0	0.0
0.0000E	0 2.2	4.3	8.7	0.0	0.0
0.0000E	0 2.1	4.3	8.7	0.0	0.0
0.0000E	0 2.1	4.3	8.7	0.0	0.0
0.0000E	0 2.0	4.3	8.7	0.0	0.0
0.0000E	0 2.0	4.3	8.7	0.0	0.0

BUOY: 6003 DATE ACQUIRED: 2- 9-78 21Z

SEA DISP.	SPEC. PERIOD	LOW FREQ. WAVE HT.	LOW FREQ. WAVE PD.	HIGH FREQ. WAVE HT.	HIGH FREQ. WAVE PD.
0.0000E	0100.0	0.0	0.0	5.1	9.3
0.0000E	0 50.0	0.0	0.0	5.1	9.3
0.0000E	0 33.3	0.0	0.0	5.1	9.3
0.0000E	0 25.0	0.0	0.0	5.1	9.3
0.5560E	-5 20.0	0.0	20.0	5.1	9.3
0.7463E	1 16.7	0.8	16.7	5.1	9.3
0.6905E	1 14.3	1.3	15.8	5.0	9.3
0.4920E	2 12.5	2.5	13.8	4.9	9.1
0.3732E	2 11.1	3.6	12.5	4.4	8.7
0.1817E	2 10.0	4.2	12.0	3.6	7.8
0.1245E	2 9.1	4.5	11.6	2.9	6.9
0.6724E	1 8.3	4.6	11.3	2.4	6.3
0.5537E	1 7.7	4.7	11.1	2.1	5.9
0.4351E	1 7.1	4.8	10.8	1.9	5.5
0.3165E	1 6.7	4.9	10.6	1.6	5.2
0.1979E	1 6.3	4.9	10.5	1.4	4.9
0.1675E	1 5.9	5.0	10.4	1.3	4.6
0.1372E	1 5.6	5.0	10.3	1.2	4.5
0.1068E	1 5.3	5.0	10.2	1.1	4.3
0.7649E	0 5.0	5.0	10.1	1.0	4.1
0.6749E	0 4.8	5.0	10.0	0.9	4.0
0.5930E	0 4.5	5.0	9.9	0.8	3.9
0.5070E	0 4.3	5.1	9.9	0.7	3.8
0.4210E	0 4.2	5.1	9.8	0.7	3.7
0.3853E	0 4.0	5.1	9.7	0.6	3.6
0.3495E	0 3.8	5.1	9.7	0.6	3.5
0.3137E	0 3.7	5.1	9.6	0.5	3.4
0.2780E	0 3.6	5.1	9.6	0.5	3.4
0.2490E	0 3.4	5.1	9.5	0.4	3.3
0.2201E	0 3.3	5.1	9.5	0.4	3.2
0.1911E	0 3.2	5.1	9.4	0.3	3.2
0.1622E	0 3.1	5.1	9.4	0.3	3.1
0.1333E	0 3.0	5.1	9.4	0.2	3.1
0.0000E	0 2.9	5.1	9.3	0.1	3.0
0.0000E	0 2.9	5.1	9.3	0.0	0.0
0.0000E	0 2.8	5.1	9.3	0.0	0.0
0.0000E	0 2.7	5.1	9.3	0.0	0.0
0.0000E	0 2.6	5.1	9.3	0.0	0.0
0.0000E	0 2.6	5.1	9.3	0.0	0.0
0.0000E	0 2.5	5.1	9.3	0.0	0.0
0.0000E	0 2.4	5.1	9.3	0.0	0.0
0.0000E	0 2.4	5.1	9.3	0.0	0.0
0.0000E	0 2.3	5.1	9.3	0.0	0.0
0.0000E	0 2.3	5.1	9.3	0.0	0.0
0.0000E	0 2.2	5.1	9.3	0.0	0.0
0.0000E	0 2.2	5.1	9.3	0.0	0.0
0.0000E	0 2.1	5.1	9.3	0.0	0.0
0.0000E	0 2.1	5.1	9.3	0.0	0.0
0.0000E	0 2.0	5.1	9.3	0.0	0.0
0.0000E	0 2.0	5.1	9.3	0.0	0.0

BUOY: 6003 DATE ACQUIRED: 2-10-78 03

SEA DISP.	SPEC. PERIOD	LOW FREQ. WAVE HT.	LOW FREQ. WAVE PD.	HIGH FREQ. WAVE HT.	HIGH FREQ. WAVE PD.
0.0000E	0100.0	0.0	0.0	3.5	8.7
0.0000E	0 50.0	0.0	0.0	3.5	8.7
0.0000E	0 33.3	0.0	0.0	3.5	8.7
0.0000E	0 25.0	0.0	0.0	3.5	8.7
0.2804E	-5 20.0	0.0	20.0	3.5	8.7
0.3764E	1 16.7	0.5	16.7	3.5	8.7
0.1889E	1 14.3	0.9	16.1	3.5	8.6
0.7938E	1 12.5	1.2	14.1	3.4	8.5
0.2977E	2 11.1	2.1	12.1	3.3	8.3
0.7477E	1 10.0	2.7	11.6	2.8	7.6
0.5839E	1 9.1	2.9	11.3	2.2	6.7
0.4192E	1 8.3	3.0	10.9	1.9	6.3
0.3508E	1 7.7	3.1	10.7	1.7	5.9
0.2820E	1 7.1	3.2	10.4	1.5	5.6
0.2134E	1 6.7	3.3	10.2	1.4	5.3
0.1944E	1 6.3	3.3	10.0	1.2	5.0
0.1754E	1 5.9	3.4	9.8	1.1	4.7
0.1436E	1 5.6	3.4	9.7	1.0	4.5
0.8208E	0 5.3	3.4	9.5	0.9	4.4
0.6116E	0 5.0	3.4	9.4	0.8	4.2
0.5199E	0 4.8	3.4	9.3	0.7	4.0
0.4282E	0 4.5	3.4	9.2	0.6	3.9
0.3365E	0 4.3	3.5	9.2	0.5	3.8
0.2448E	0 4.2	3.5	9.1	0.5	3.6
0.2170E	0 4.0	3.5	9.0	0.5	3.5
0.1892E	0 3.8	3.5	9.0	0.4	3.5
0.1615E	0 3.7	3.5	8.9	0.4	3.4
0.1336E	0 3.6	3.5	8.9	0.4	3.3
0.1265E	0 3.4	3.5	8.9	0.3	3.3
0.1194E	0 3.3	3.5	8.8	0.3	3.2
0.1123E	0 3.2	3.5	8.8	0.3	3.2
0.1052E	0 3.1	3.5	8.7	0.2	3.1
0.1051E	0 3.0	3.5	8.7	0.2	3.1
0.0000E	0 2.9	3.5	8.7	0.0	3.0
0.0000E	0 2.9	3.5	8.7	0.0	0.0
0.0000E	0 2.8	3.5	8.7	0.0	0.0
0.0000E	0 2.7	3.5	8.7	0.0	0.0
0.0000E	0 2.6	3.5	8.7	0.0	0.0
0.0000E	0 2.6	3.5	8.7	0.0	0.0
0.0000E	0 2.5	3.5	8.7	0.0	0.0
0.0000E	0 2.4	3.5	8.7	0.0	0.0
0.0000E	0 2.4	3.5	8.7	0.0	0.0
0.0000E	0 2.3	3.5	8.7	0.0	0.0
0.0000E	0 2.3	3.5	8.7	0.0	0.0
0.0000E	0 2.2	3.5	8.7	0.0	0.0
0.0000E	0 2.2	3.5	8.7	0.0	0.0
0.0000E	0 2.1	3.5	8.7	0.0	0.0
0.0000E	0 2.1	3.5	8.7	0.0	0.0
0.0000E	0 2.0	3.5	8.7	0.0	0.0

217 S FEB 78 51.312N 158.821W

WIND DIR 297.5 WIND SPD 15.8 WHITE CPS 1 USTR .57

FREQ	.164	.153	.133	.117	.103	.091	.083	.078	.072	.067	.061	.056	.050	.044	.039		DIR(FROM)
	.050	.050	0.000	0.000	0.000	0.000	0.000	0.000	0.000	0.000	0.000	0.000	0.000	0.000	0.000	.140	337.5
	.080	.100	0.000	.070	.010	0.000	.010	0.000	0.000	0.000	0.000	0.000	0.000	0.000	0.000	.290	292.5
	.030	.050	.060	0.000	0.000	0.000	0.000	.010	.010	.010	.010	0.000	0.000	0.000	0.000	.140	247.5
	.020	.010	0.000	0.000	0.000	0.000	.010	.040	.020	.030	.010	0.000	0.000	0.000	0.000	.150	202.5
	0.000	0.000	0.000	0.000	0.000	0.000	.010	.030	.020	.010	0.000	0.000	0.000	0.000	0.000	.070	157.5
	0.000	0.000	0.000	0.000	0.000	0.000	0.000	0.000	0.000	0.000	0.000	0.000	0.000	0.000	0.000	0.000	112.5
	0.000	0.000	0.000	0.000	0.000	0.000	0.000	0.000	0.000	0.000	0.000	0.000	0.000	0.000	0.000	0.000	67.5
	0.000	0.000	0.000	0.000	0.000	0.000	0.000	0.000	0.000	0.000	0.000	0.000	0.000	0.000	0.000	0.000	22.5
	0.000	0.000	0.000	0.000	0.000	0.000	0.000	0.000	0.000	0.000	0.000	0.000	0.000	0.000	0.000	0.000	337.5
	0.000	0.000	0.000	0.000	.010	.010	0.000	0.000	0.000	0.000	0.000	0.000	0.000	0.000	0.000	.020	292.5
	0.000	0.000	.030	.070	.170	.140	.110	.080	0.000	0.000	0.000	0.000	0.000	0.000	0.000	.600	247.5
	.030	.040	.240	.250	.310	.210	.100	0.000	0.000	0.000	0.000	0.000	0.000	0.000	0.000	1.220	202.5
	.190	.290	.370	.390	.490	.360	.250	.170	.050	.050	.020	0.000	0.000	0.000	0.000	2.630	

H1/3 6.49FT

N 37 10 FEB 78 51.312N 158.821W

WIND DIR 50.5 WIND SPD 25.0 WHITE CPS 0 USTR 0.00

FREQ	.164	.153	.133	.117	.103	.091	.083	.078	.072	.067	.061	.056	.050	.044	.039		DIR(FROM)
	0.000	0.000	0.000	0.000	0.000	0.000	0.000	0.000	0.000	0.000	0.000	0.000	0.000	0.000	0.000	0.000	337.5
	0.000	0.000	0.000	.010	0.000	0.000	.010	0.000	0.000	0.000	0.000	0.000	0.000	0.000	0.000	.020	292.5
	0.000	0.000	.010	0.000	0.000	0.000	0.000	.010	.010	.010	.010	0.000	0.000	0.000	0.000	.050	247.5
	0.000	0.000	0.000	0.000	.010	.010	.020	.050	.030	.030	.010	0.000	0.000	0.000	0.000	.160	202.5
	0.000	0.000	.010	0.000	.010	.010	.010	.030	.030	.010	0.000	0.000	0.000	0.000	0.000	.110	157.5
	.010	0.000	0.000	0.000	0.000	.050	0.000	0.000	0.000	0.000	0.000	0.000	0.000	0.000	0.000	.030	112.5
	.030	0.000	0.000	0.000	0.000	0.000	0.000	0.000	0.000	0.000	0.000	0.000	0.000	0.000	0.000	.030	67.5
	.040	0.000	0.000	0.000	0.000	0.000	0.000	0.000	0.000	0.000	0.000	0.000	0.000	0.000	0.000	.040	22.5
	.030	0.000	0.000	0.000	0.000	0.000	0.000	0.000	0.000	0.000	0.000	0.000	0.000	0.000	0.000	.030	337.5
	.010	0.000	0.000	0.000	0.000	.010	.010	.010	0.000	0.000	0.000	0.000	0.000	0.000	0.000	.040	292.5
	0.000	0.000	.010	.050	.110	.090	.060	.060	0.000	0.000	0.000	0.000	0.000	0.000	0.000	.400	247.5
	0.000	0.000	.050	.090	.120	.090	.060	0.000	0.000	0.000	0.000	0.000	0.000	0.000	0.000	.410	202.5
	.120	0.000	.080	.150	.250	.260	.190	.160	.070	.050	.020	0.000	0.000	0.000	0.000	1.350	

H1/3 4.65FT

Table B-2.1 SOWM Data Output, Grid Pt. 51.3N, 158.8W.

21Z 9 FEB 78 54.395N 158.057W

WIND DIR 336.9 WIND SPD 22.5 WHITE CPS 3 USTR .90

FREQ	.164	.153	.133	.117	.103	.091	.083	.078	.072	.067	.061	.056	.050	.044	.039		DIR(FROM)
	.060	.180	.250	.210	0.000	.180	.020	0.000	0.000	0.000	0.000	0.000	0.000	0.000	0.000	.900	309.9
	.040	.100	.130	.080	.150	.090	0.000	0.000	.010	0.000	0.000	0.000	0.000	0.000	0.000	.600	279.9
	0.000	0.000	0.000	0.000	0.000	0.000	0.000	0.000	0.000	0.000	0.000	0.000	0.000	0.000	0.000	0.000	249.9
	0.000	0.000	0.000	0.000	0.000	0.000	0.000	0.000	.010	0.000	0.000	0.000	0.000	0.000	0.000	.010	219.9
	0.000	0.000	0.000	0.000	0.000	0.000	0.000	.020	.010	.010	0.000	0.000	0.000	0.000	0.000	.040	189.9
	0.000	0.000	0.000	0.000	0.000	0.000	0.000	0.000	0.000	0.000	0.000	0.000	0.000	0.000	0.000	0.000	159.9
	0.000	0.000	0.000	0.000	0.000	0.000	0.000	0.000	0.000	0.000	0.000	0.000	0.000	0.000	0.000	0.000	129.9
	0.000	0.000	0.000	0.000	0.000	0.000	0.000	0.000	0.000	0.000	0.000	0.000	0.000	0.000	0.000	0.000	99.9
	0.000	0.000	0.000	0.000	0.000	0.000	0.000	0.000	0.000	0.000	0.000	0.000	0.000	0.000	0.000	0.000	69.9
	.030	.070	.040	.060	0.000	0.000	0.000	0.000	0.000	0.000	0.000	0.000	0.000	0.000	0.000	.200	39.9
	.050	.140	.230	.190	.210	0.000	0.000	0.000	0.000	0.000	0.000	0.000	0.000	0.000	0.000	.820	9.9
	.060	.210	.320	.280	0.000	0.000	0.000	0.000	0.000	0.000	0.000	0.000	0.000	0.000	0.000	.870	339.9
	.240	.700	1.010	.820	.360	.270	.020	.020	.030	.010	0.000	0.000	0.000	0.000	0.000	3.480	

H1/3 7.46FT

3Z 10 FEB 78 54.395N 158.067W

WIND DIR 344.9 WIND SPD 18.5 WHITE CPS 2 USTR .68

FREQ	.164	.153	.133	.117	.103	.091	.083	.078	.072	.067	.061	.056	.050	.044	.039		DIR(FROM)
	.040	.110	.120	.140	.030	.050	0.000	0.000	0.000	0.000	0.000	0.000	0.000	0.000	0.000	.590	309.9
	.020	.040	.100	.040	.050	.070	0.000	0.000	.010	0.000	0.000	0.000	0.000	0.000	0.000	.330	279.9
	0.000	0.000	0.000	0.000	0.000	0.000	0.000	0.000	0.000	0.000	0.000	0.000	0.000	0.000	0.000	0.000	249.9
	0.000	0.000	0.000	0.000	0.000	0.000	0.000	0.000	.020	0.000	0.000	0.000	0.000	0.000	0.000	.020	219.9
	0.000	0.000	0.000	0.000	0.000	0.000	0.000	.020	.020	.010	0.000	0.000	0.000	0.000	0.000	.050	189.9
	0.000	0.000	0.000	0.000	0.000	0.000	0.000	0.000	0.000	0.000	0.000	0.000	0.000	0.000	0.000	0.000	159.9
	0.000	0.000	0.000	0.000	0.000	0.000	0.000	0.000	0.000	0.000	0.000	0.000	0.000	0.000	0.000	0.000	129.9
	0.000	0.000	0.000	0.000	0.000	0.000	0.000	0.000	0.000	0.000	0.000	0.000	0.000	0.000	0.000	0.000	99.9
	0.000	0.000	0.000	0.000	0.000	0.000	0.000	0.000	.010	0.000	0.000	0.000	0.000	0.000	0.000	.010	69.9
	.040	.100	.110	.050	0.000	0.000	0.000	0.000	0.000	0.000	0.000	0.000	0.000	0.000	0.000	.300	39.9
	.060	.190	.230	.120	.060	0.000	0.000	0.000	0.000	0.000	0.000	0.000	0.000	0.000	0.000	.660	9.9
	.060	.190	.240	.110	0.000	0.000	0.000	0.000	0.000	0.000	0.000	0.000	0.000	0.000	0.000	.600	339.9
	.220	.630	.860	.660	.140	.160	0.000	.020	.060	.010	0.000	0.000	0.000	0.000	0.000	2.560	

H1/3 6.40FT

Table B-2.2 SOWM Data Output, Grid Pt. 54.4N, 158.0W.

21Z 9 FEB 78 49.299N 155.094W

WIND DIR 291.3 WIND SPD 25.3 WHITE CPS 4 USTR 1.01

FREQ .144	.153	.133	.117	.103	.091	.083	.074	.072	.067	.061	.056	.050	.044	.039		DIR(FROM)
.050	.180	.370	.330	.480	.470	0.000	.030	0.000	0.000	0.000	0.000	0.000	0.000	0.000	1.910	312.30
.060	.210	.300	.330	0.000	.440	.290	.190	0.000	0.000	0.000	0.000	0.000	0.000	0.000	1.820	282.30
.050	.160	.160	.210	0.000	.040	.070	.040	.050	.030	.020	0.000	0.000	0.000	0.000	.830	252.30
.030	.090	.130	.100	.120	.050	.030	.060	.060	.040	.020	0.000	0.000	0.000	0.000	.730	222.30
0.000	0.000	0.000	0.000	0.000	0.000	0.000	0.000	.030	.010	.010	0.000	0.000	0.000	0.000	.050	192.30
0.000	0.000	.010	.010	0.000	0.000	0.000	0.000	0.000	0.000	0.000	0.000	0.000	0.000	0.000	.020	162.30
0.000	0.000	0.000	0.000	0.000	0.000	0.000	0.000	0.000	0.000	0.000	0.000	0.000	0.000	0.000	0.000	132.30
0.000	0.000	0.000	0.000	0.000	0.000	0.000	0.000	0.000	0.000	0.000	0.000	0.000	0.000	0.000	0.000	102.30
0.000	0.000	0.000	0.000	0.000	0.000	0.000	0.000	0.000	0.000	0.000	0.000	0.000	0.000	0.000	0.000	72.30
0.000	0.000	0.000	0.000	0.000	0.000	0.000	0.000	0.000	0.000	0.000	0.000	0.000	0.000	0.000	0.000	42.30
0.000	0.000	0.000	.360	.720	.470	.160	.100	.040	.010	.010	0.000	0.000	0.000	0.000	1.750	12.30
.030	.160	.360	.360	.490	.470	.430	.330	.100	.140	0.000	0.000	0.000	0.000	0.000	2.650	342.30
.220	.740	1.330	1.700	1.810	1.840	.960	.750	.280	.270	.060	0.000	0.000	0.000	0.000	9.960	

H1/3 12.42FT

3Z 10 FEB 78 49.299N 155.094W

WIND DIR 253.3 WIND SPD 13.4 WHITE CPS 1 USTR .48

FREQ .144	.153	.133	.117	.103	.091	.083	.074	.072	.067	.061	.056	.050	.044	.039		DIR(FROM)
0.000	0.000	.020	.080	.140	.260	.010	.030	0.000	0.000	0.000	0.000	0.000	0.000	0.000	.540	312.30
.010	0.000	.250	.250	0.000	.280	.080	.020	0.000	0.000	0.000	0.000	0.000	0.000	0.000	.690	282.30
.030	.020	.130	.200	0.000	.040	.020	.060	.050	.030	.010	0.000	0.000	0.000	0.000	.500	252.30
.050	.050	.130	.080	.050	.040	.060	.060	.070	.040	.020	0.000	0.000	0.000	0.000	.690	222.30
.050	.040	0.000	0.000	0.000	.010	0.000	.010	.040	.010	.010	0.000	0.000	0.000	0.000	.170	192.30
.020	.020	0.000	0.000	0.000	0.000	0.000	0.000	0.000	0.000	0.000	0.000	0.000	0.000	0.000	.040	162.30
0.000	0.000	0.000	0.000	0.000	0.000	0.000	0.000	0.000	0.000	0.000	0.000	0.000	0.000	0.000	0.000	132.30
0.000	0.000	0.000	0.000	0.000	0.000	0.000	0.000	0.000	0.000	0.000	0.000	0.000	0.000	0.000	0.000	102.30
0.000	0.000	0.000	0.000	0.000	0.000	0.000	0.000	0.000	0.000	0.000	0.000	0.000	0.000	0.000	0.000	72.30
0.000	0.000	0.000	0.000	0.000	0.000	0.000	0.000	0.000	0.000	0.000	0.000	0.000	0.000	0.000	0.000	42.30
0.000	0.000	.010	0.000	.040	.100	.060	.060	.020	.010	.010	0.000	0.000	0.000	0.000	.320	12.30
0.000	0.000	0.000	.010	.040	.120	.170	.160	.060	.120	0.000	0.000	0.000	0.000	0.000	.720	342.30
.160	.130	.530	.620	.420	.850	.370	.400	.240	.210	.050	0.000	0.000	0.000	0.000	3.950	

H1/3 7.98FT

Table B-2.3 SOWM Data Output, Grid Pt. 49.3N, 155.1W.

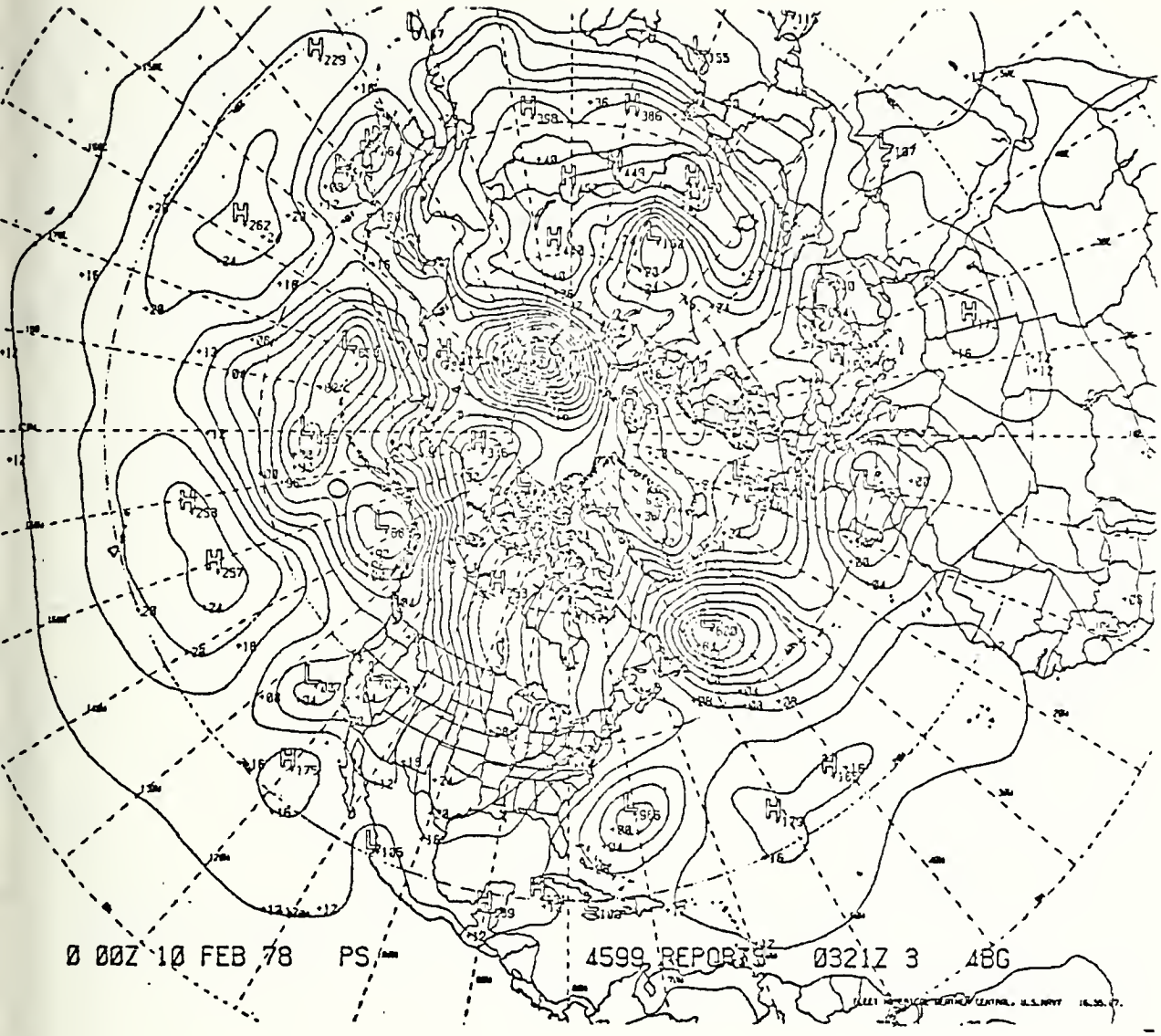

Figure B.-1 FNWC Northern Hemispheric Surface Pressure, 00Z 10 Feb 78.

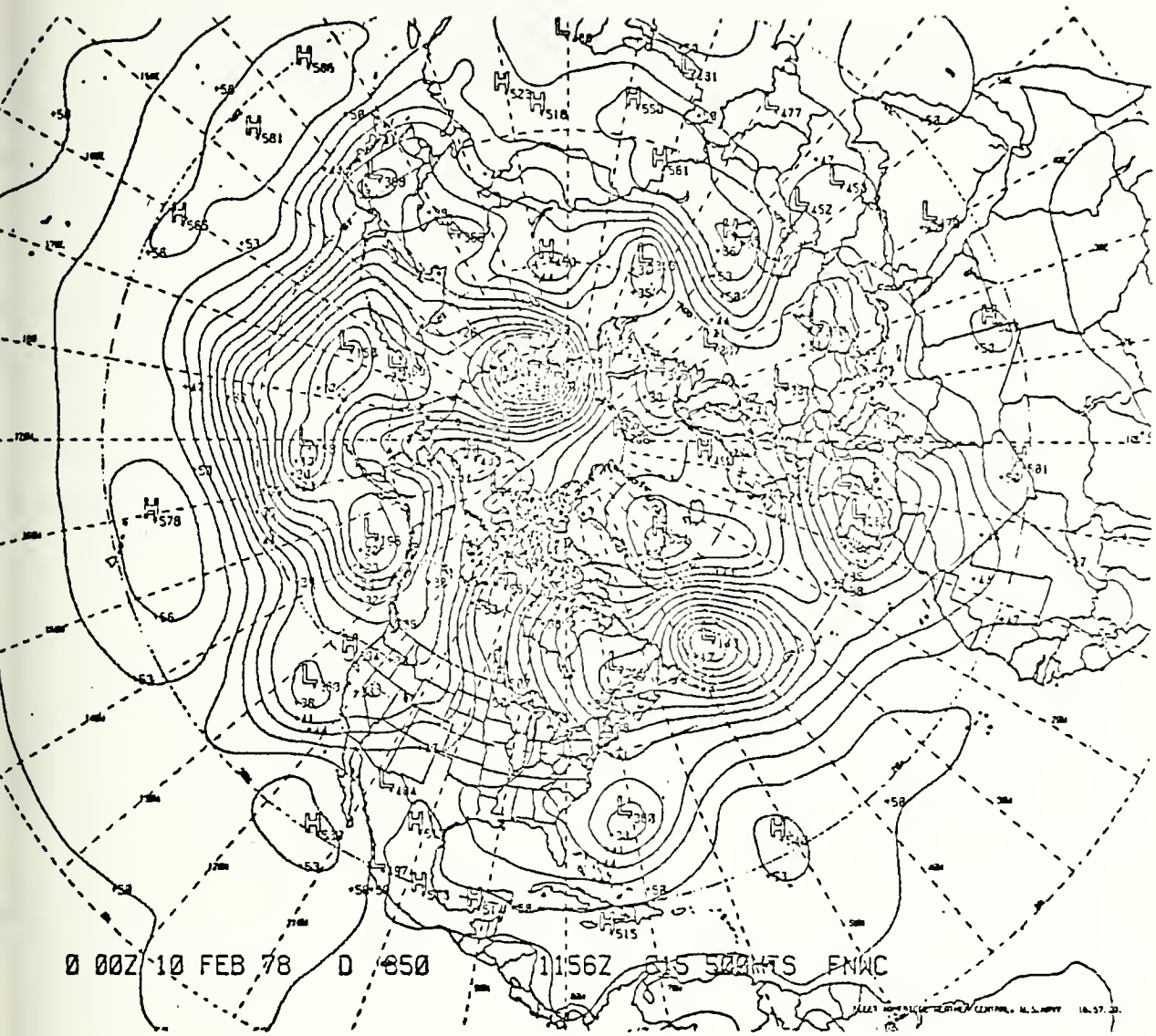

Figure B.-2 FNWC Northern Hemispheric 850mb Heights, 00Z 10 Feb 78.

APPENDIX C
DERIVATION OF SURFACE WAVE FREQUENCY SHIFT DUE TO MOTION OF AIRCRAFT RELATIVE TO THE WAVE

The wave equation due to motion of the aircraft is,

$$e^{i\omega t - mx'} = e^{i\omega' t - mx}$$

Where ω is the angular frequency of the wave, m is the wave number, t is the time and x is the distance from a refrence point in the direction of wave propagation. The primed terms are the values due to motion,

$$x' = x + (u\cos\psi)t$$

Where u is the aircraft velocity and ψ is the angle clockwise from the horizontal wave motion vector to the horizontal aircraft motion vector.

Then,

$$e^{i\omega t - m(x+(u\cos\psi)t)} = e^{i\omega' t - mx}$$

which leads to

$$e^{i\omega t - mu(\cos\psi)t} = e^{i\omega' t}$$

then solving for ω' leads to

$$\omega' = \omega - mu\cos\psi$$

when $\omega = {}^{2\pi}/_{f}$, $m = {}^{2\pi}/_{L}$ and $L = {}^{gT^2}/_{2\pi}$,

equation 26 results

$$f' = f\left[1 - {}^{2\pi fu}/_{g}\cos\psi\right] \qquad (26)$$

APPENDIX D
SPECTRAL VALUES OF AIRCRAFT DATA AND MODELED NOISE

I. MAGNETIC CONSTANTS AT 52N, 156N FOR FEBRUARY 1978

Earth's total magnetic field, B_e = 50,807 nT

Dip angle, $I = 20^{\circ}$

THE MODELED MAGNETIC NOISE PRODUCED FROM
THE PREDICTED SOWM SPECTRA DATA LEG 1

FREQUENCY (Hz)	AMPLITUDE ($^{n}T^{2}$/Hz)
.012	.0002
.03	.0002
.12	.0024
.14	.0037
.16	.0029
.18	.0041
.20	.0014
.22	.0001
.23	.00064
.26	.0015
.27	.0028
.29	.0102
.32	.0039
.36	.0041
.37	.0076
.42	.0128
.45	.0048
.47	.0054
.56	.0052
.7	.0016
.91	.0018
1.1	.00002

Table D-1.a The Modeled Magnetic Noise Produced From the Predicted SOWM Data, Aircraft Course 270°.

FREQUENCY (Hz)	AMPLITUDE (nT^2/Hz)
.11	.00087
.13	.0012
.14	.0012
.16	.0037
.18	.0015
.21	.0014
.25	.0013
.27	.0057
.28	.0088
.31	.00004
.32	.0087
.36	.0069
.37	.0063
.42	.0039
.43	.0096
.47	.0034
.53	.0012
.56	.0022
.68	.0002
.7	.00057
.89	.00019
.9	.00018
1.13	.000018

Table D-1.b The Modeled Magnetic Noise Produced From the Predicted SOWM Data, Aircarft Course 000^{o}.

Table D-2 FFT Numerical Output of Aircraft Data (Course 270°).

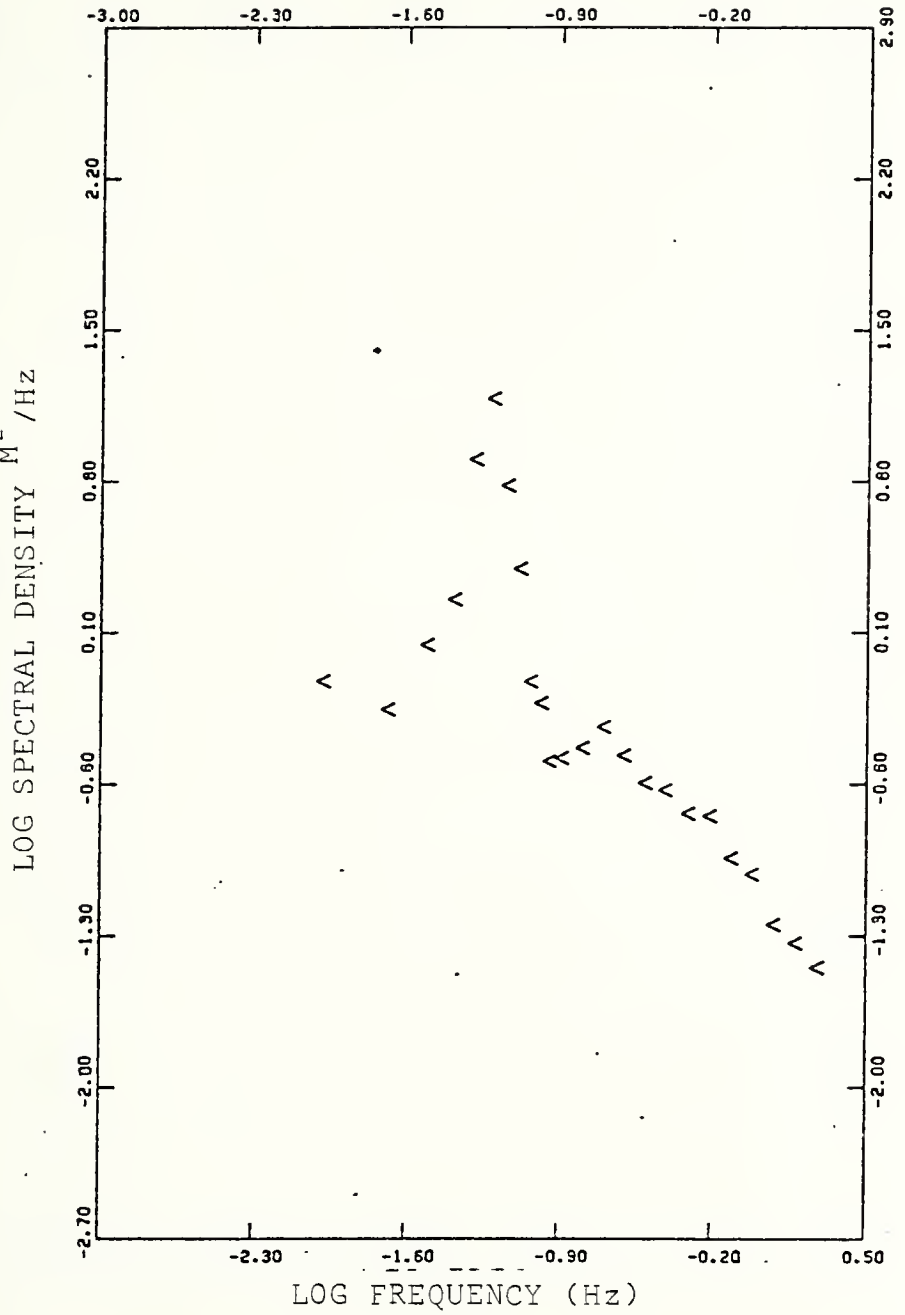

Figure D-1 Altitude Spectrum (CS 000°).

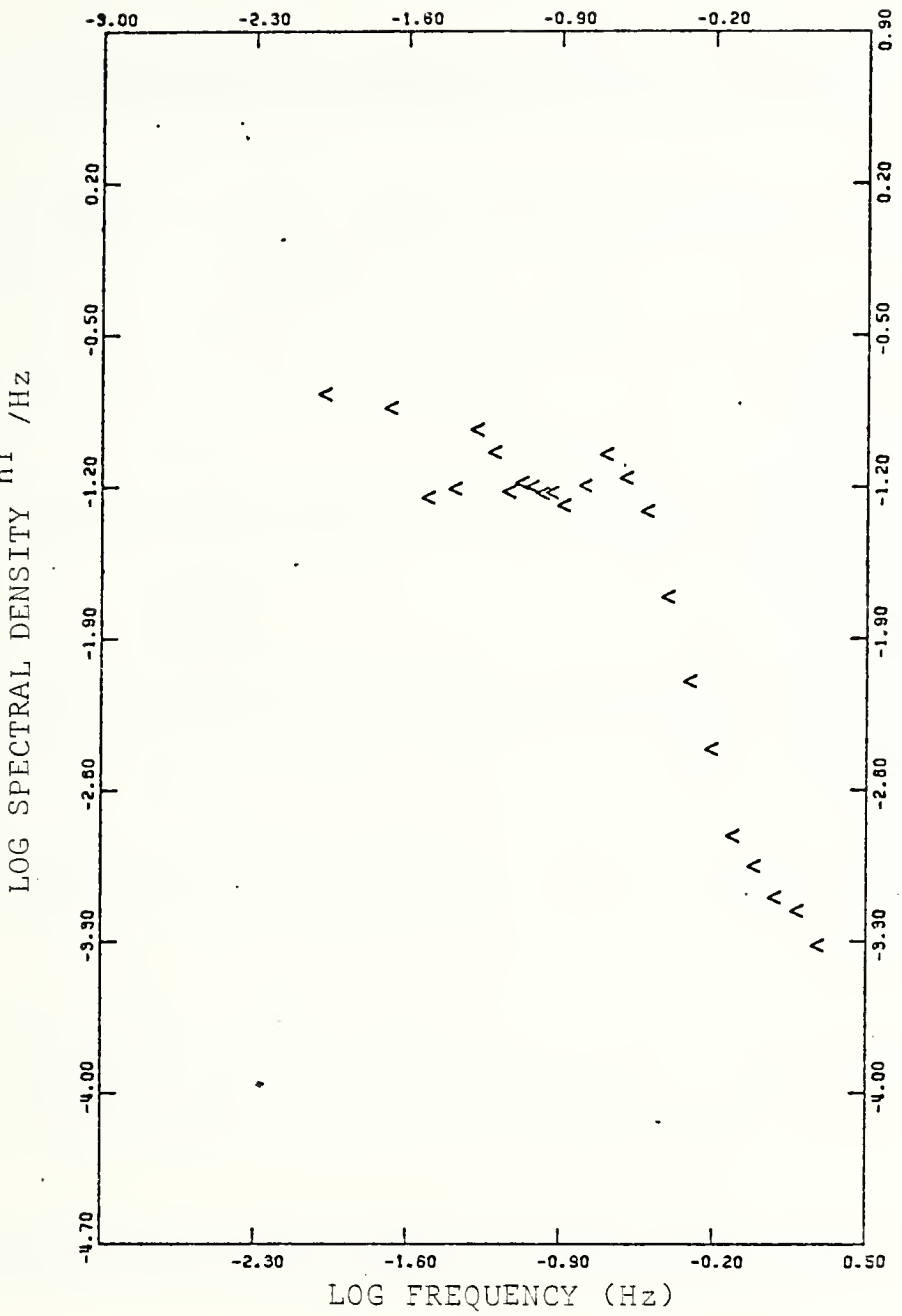

Figure D-2 Magnetic Spectrum (CS 000°).

FREQUENCY	AUTO-SPECTRUM	ALTU-SPECTRUM	CC-SPECTRUM	QUAD-SPECTRUM	WAVE FEPICO	PHASE	COHERENCE
0.0	0.1103452E-02	0.1103452E-02	0.1854312E-02	0.0	0.0	0.0	0.823354
0.0195313	0.1452266E-02	0.1452266E-02	0.1834576E-02	0.1762626E-01	102.3556	1.515558	0.715543
0.0390625	0.3539994E-02	0.3539994E-02	0.2547445E-02	-0.5525508E-01	11.15558	0.1946234	0.611550
0.0585938	0.8150810E-02	0.8150810E-02	0.1177217E-02	-0.1133932	2.113332	0.1982773	0.421149
0.0781250	0.1672016E-01	0.1672016E-01	-0.2103164E-01	-0.1559959	0.5559959	1.570796	0.064964
0.0976563	0.3477596E-01	0.3477596E-01	-0.3512503E-01	-0.1955650	0.2955650	1.570796	0.071174
0.1171875	0.6437575E-01	0.6437575E-01	-0.4343216E-01	-0.2345273	0.1345273	1.570796	0.064302
0.1367188	0.1026414E+00	0.1026414E+00	-0.4263113E-01	-0.2734727	0.1345273	1.570796	0.064302
0.1562500	0.1452266E+00	0.1452266E+00	-0.3032422E-01	-0.3124180	0.1345273	1.570796	0.064302
0.1757813	0.1870156E+00	0.1870156E+00	-0.1709771E-01	-0.3513633	0.1345273	1.570796	0.064302
0.1953125	0.2247715E+00	0.2247715E+00	-0.2165257E-02	-0.3903086	0.1345273	1.570796	0.064302
0.2148438	0.2577902E+00	0.2577902E+00	0.1130562E-01	-0.4292539	0.1345273	1.570796	0.064302
0.2343750	0.2855955E+00	0.2855955E+00	0.2067116E-01	-0.4681992	0.1345273	1.570796	0.064302
0.2539063	0.3077761E+00	0.3077761E+00	0.2912144E-01	-0.5071445	0.1345273	1.570796	0.064302
0.2734375	0.3240615E+00	0.3240615E+00	0.3665166E-01	-0.5460898	0.1345273	1.570796	0.064302
0.2929688	0.3343233E+00	0.3343233E+00	0.4326277E-01	-0.5850351	0.1345273	1.570796	0.064302
0.3125000	0.3385744E+00	0.3385744E+00	0.4895476E-01	-0.6239804	0.1345273	1.570796	0.064302
0.3320313	0.3369674E+00	0.3369674E+00	0.5372764E-01	-0.6629257	0.1345273	1.570796	0.064302
0.3515625	0.3297771E+00	0.3297771E+00	0.5758141E-01	-0.7018710	0.1345273	1.570796	0.064302
0.3710938	0.3174176E+00	0.3174176E+00	0.6051606E-01	-0.7408163	0.1345273	1.570796	0.064302
0.3906250	0.3003069E+00	0.3003069E+00	0.6253160E-01	-0.7797616	0.1345273	1.570796	0.064302
0.4101563	0.2788646E+00	0.2788646E+00	0.6362803E-01	-0.8187069	0.1345273	1.570796	0.064302
0.4296875	0.2535124E+00	0.2535124E+00	0.6380534E-01	-0.8576522	0.1345273	1.570796	0.064302
0.4492188	0.2246715E+00	0.2246715E+00	0.6306354E-01	-0.8965975	0.1345273	1.570796	0.064302
0.4687500	0.1927615E+00	0.1927615E+00	0.6140263E-01	-0.9355428	0.1345273	1.570796	0.064302
0.4882813	0.1582000E+00	0.1582000E+00	0.5882260E-01	-0.9744881	0.1345273	1.570796	0.064302
0.5078125	0.1213999E+00	0.1213999E+00	0.5532346E-01	-0.1013433	0.1345273	1.570796	0.064302
0.5273438	0.8277116E-01	0.8277116E-01	0.5090521E-01	-0.1052379	0.1345273	1.570796	0.064302
0.5468750	0.4283600E-01	0.4283600E-01	0.4556784E-01	-0.1091324	0.1345273	1.570796	0.064302
0.5664063	0.1203600E-01	0.1203600E-01	0.3931136E-01	-0.1130270	0.1345273	1.570796	0.064302
0.5859375	0.1203600E-01	0.1203600E-01	0.3213577E-01	-0.1169215	0.1345273	1.570796	0.064302
0.6054688	0.4283600E-01	0.4283600E-01	0.2404106E-01	-0.1208161	0.1345273	1.570796	0.064302
0.6250000	0.8277116E-01	0.8277116E-01	0.1502724E-01	-0.1247106	0.1345273	1.570796	0.064302
0.6445313	0.1213999E+00	0.1213999E+00	0.5094309E-02	-0.1286052	0.1345273	1.570796	0.064302
0.6640625	0.1582000E+00	0.1582000E+00	-0.5849333E-02	-0.1324997	0.1345273	1.570796	0.064302
0.6835938	0.1927615E+00	0.1927615E+00	-0.1774299E-01	-0.1363943	0.1345273	1.570796	0.064302
0.7031250	0.2246715E+00	0.2246715E+00	-0.2963665E-01	-0.1402888	0.1345273	1.570796	0.064302
0.7226563	0.2535124E+00	0.2535124E+00	-0.4153031E-01	-0.1441834	0.1345273	1.570796	0.064302
0.7421875	0.2788646E+00	0.2788646E+00	-0.5342397E-01	-0.1480779	0.1345273	1.570796	0.064302
0.7617188	0.3003069E+00	0.3003069E+00	-0.6531763E-01	-0.1519725	0.1345273	1.570796	0.064302
0.7812500	0.3174176E+00	0.3174176E+00	-0.7721129E-01	-0.1558670	0.1345273	1.570796	0.064302
0.8007813	0.3297771E+00	0.3297771E+00	-0.8910495E-01	-0.1597616	0.1345273	1.570796	0.064302
0.8203125	0.3369674E+00	0.3369674E+00	-0.1009986E+00	-0.1636561	0.1345273	1.570796	0.064302
0.8398438	0.3385744E+00	0.3385744E+00	-0.1128923E+00	-0.1675507	0.1345273	1.570796	0.064302
0.8593750	0.3343233E+00	0.3343233E+00	-0.1247859E+00	-0.1714452	0.1345273	1.570796	0.064302
0.8789063	0.3240615E+00	0.3240615E+00	-0.1366796E+00	-0.1753398	0.1345273	1.570796	0.064302
0.8984375	0.3077761E+00	0.3077761E+00	-0.1485732E+00	-0.1792343	0.1345273	1.570796	0.064302
0.9179688	0.2855955E+00	0.2855955E+00	-0.1604669E+00	-0.1831289	0.1345273	1.570796	0.064302
0.9375000	0.2577902E+00	0.2577902E+00	-0.1723605E+00	-0.1870234	0.1345273	1.570796	0.064302
0.9570313	0.2247715E+00	0.2247715E+00	-0.1842542E+00	-0.1909180	0.1345273	1.570796	0.064302
0.9765625	0.1870156E+00	0.1870156E+00	-0.1961478E+00	-0.1948125	0.1345273	1.570796	0.064302
0.9960938	0.1452266E+00	0.1452266E+00	-0.2080415E+00	-0.1987071	0.1345273	1.570796	0.064302
1.0156250	0.1026414E+00	0.1026414E+00	-0.2199351E+00	-0.2026016	0.1345273	1.570796	0.064302
1.0351563	0.6437575E-01	0.6437575E-01	-0.2318288E+00	-0.2064962	0.1345273	1.570796	0.064302
1.0546875	0.3477596E-01	0.3477596E-01	-0.2437224E+00	-0.2103907	0.1345273	1.570796	0.064302
1.0742188	0.1672016E-01	0.1672016E-01	-0.2556161E+00	-0.2142853	0.1345273	1.570796	0.064302
1.0937500	0.8150810E-02	0.8150810E-02	-0.2675097E+00	-0.2181798	0.1345273	1.570796	0.064302
1.1132813	0.3539994E-02	0.3539994E-02	-0.2794034E+00	-0.2220744	0.1345273	1.570796	0.064302
1.1328125	0.1452266E-02	0.1452266E-02	-0.2912970E+00	-0.2259689	0.1345273	1.570796	0.064302
1.1523438	0.1103452E-02	0.1103452E-02	-0.3031907E+00	-0.2298635	0.1345273	1.570796	0.064302

Table -3 FFT Numerical Output of Aircraft Data (Course 270°).

4.51411	0.11433E-04	.8902669E-01	0.6218020E-04	-0.1137EE-04	0.2C5?5	-1C.2EE07	0.C0354
4.52108	0.2641136E-04	.1005E633E CO	-.1225E44C-03	0.190317E-05	0.20317	125.17773	0.C2430
4.52164	0.1716J10E-04	.9117836E-01	0.2781502E-03	0.13641F-04	0.2C377	3.AC722	0.C5556
4.52341	0.1C44221E-04	.5554454E-01	0.1428705E-03	0.10197F-03	0.2C327	25.51422	0.C2564
4.53117	0.15E2730L-04	.1197475E CO	-.2594526E-03	0.215?2E-03	0.2C147	14.51241	0.C7214
4.53454	0.1177403E-04	.1077143E CO	-.1E13E40E-03	0.19796E-03	0.2C157	125.2C154	0.J5952
4.57J7C	0.1111E464E-04	.1010569E CO	-.7943256E-04	-0.2946?E-05	0.20118	1C4.31466	0.C6762
4.5C047	0.1521226E-04	.9837750F-01	-.2610704E-04	-0.51011E-04	0.2C076	-117.1CC23	0.C3233
4.5C429	0.1431C69L-04	.1056151E CO	-.3284540E-03	0.60548F-04	0.2C029	125.45263	0.C9211
5.CCCOC	0.3211747E-05	.1356ICCE-01	-.6321456E-05	0.0	0.20000	11C.CCCCC	0.CJ361

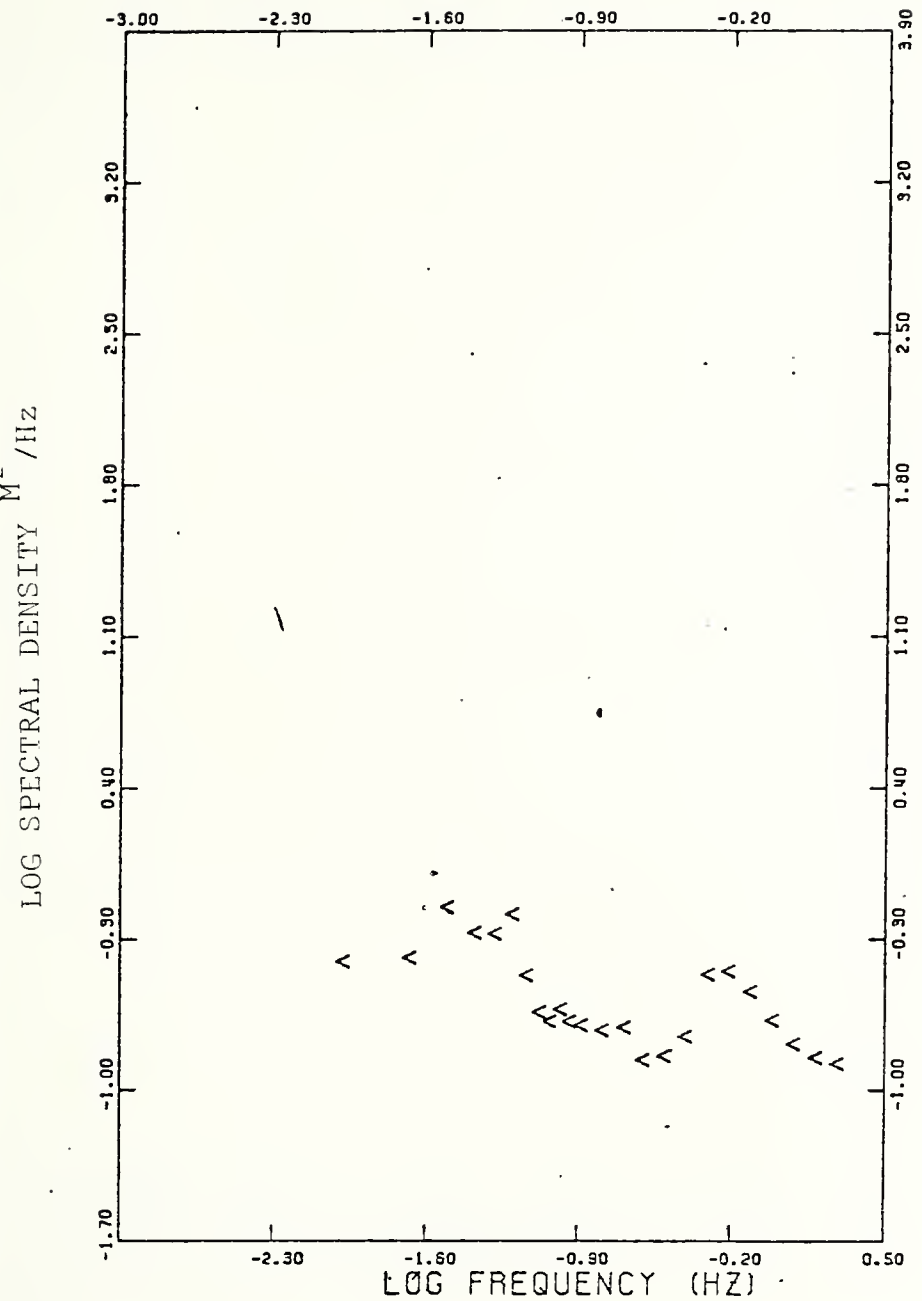

Figure D-3 Altitude Spectrum.

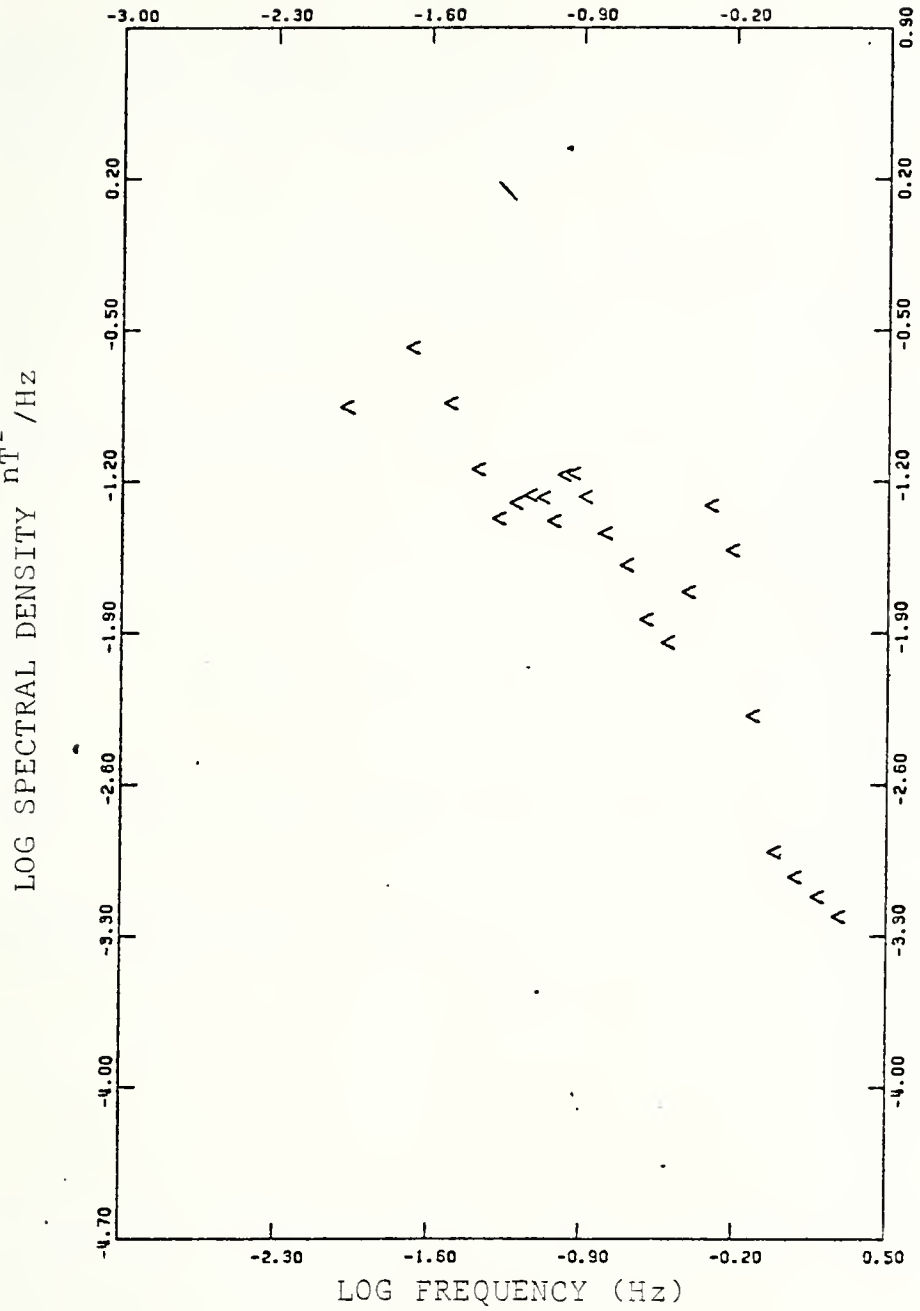

Figure D-4 Magnetic Spectrum.

LIST OF REFERENCES

Baker, R. and Graefe, P.W.U., "Ocean Wave Profile and Spectra Measurement Using an Airborne Magnetometer," National Research Council, Canada. Division of Mechanical Engineering Quarterly Bulletin, V.4, 1968.

Bendat, J. S. and Piersol, A. G., Random Data: Analysis and Measurement Procedures, John Wiley and Sons, Inc., 1971.

Dobrin, M. B., Introduction to Geophysical Prospecting, McGraw Hill, 1952.

Fleet Numerical Weather Center Technical Note No. 75-3, An Evaluation of a Hemispheric Operational Wave Spectral Model, by S. M. Lazanoff and N. M. Stevenson, June 1975.

National Oceanic and Atmospheric Admisnitration, Office of Ocean Engineering, NOAA Data Buoy Office, NDBO Wave Measurements, by K. Steele and A. Johnson, Jr., July 1977.

Silvester, R., Coastal Engineering, Elsevier Scientific Pub. Co., 1974.

Weaver, J. T., "Magnetic Variations Associated with Ocean Waves and Swell," Journal of Geophysical Research, V. 70, No. 8, p. 1921-1929, 15 April 1965.

Widrow, B., et. al., "Adaptive Noise Cancelling: Principles and Applications," Proceedings of the IEEE, V. 63, No. 12, p. 1692-1716, December 1975.

INITIAL DISTRIBUTION LIST

		No. Copies
1.	Defense Documentation Center Cameron Station Alexandria, Virginia 22314	2
2.	Library, Code 0142 Naval Postgraduate School Monterey, California 93940	2
3.	Department Chairman, Code 68 Department of Oceanography Naval Postgraduate School Monterey, California 93940	3
4.	LCDR A. B. Chace, Code 68Ch Department of Oceanography Naval Postgraduate School Monterey, California 93940	1
5.	LT James F. Etro, USN NWSED, NAF Sigonella FPO, New York 09523	3
6.	Commander Naval Oceanography Command NSTL Station, Mississippi 39529	1
7.	Office of Naval Research Code 481 NSTL Station, Mississippi 39529	1
8.	Dr. Robert E. Stevenson Scientific Liaison Office, ONR Scripps Institution of Oceanography La Jolla, California 92037	1
9.	SIO Library University of California, San Diego P.O. Box 2367 La Jolla, California 92037	1
10.	Department of Oceanography Library University of Washington Seattle, Washington 98105	1
11.	Department of Oceanography Library Oregon State University Corvallis, Oregon 97331	1

		No. Copies
12.	Commanding Officer Fleet Numerical Weather Central Monterey, California 93940	1
13.	Commanding Officer Naval Environmental Prediction Research Facility Monterey, California 93940	1
14.	Department of the Navy Commander Oceanographic System Pacific Box 1390 Pearl Harbor, Hawaii 96860	1
15.	Director Naval Oceanography Division (OP-952) Office of the Chief of Naval Operations Washington, DC 20350	1
16.	Commanding Officer NORDA NSTL Station, Mississippi 39529	1
17.	Commanding Officer Fleet Weather Central Attn: Ocean Services Box 113 Pearl Harbor, Hawaii 96860	1
18.	Mr. Jerry Batts Naval Intelligence Support Center Code 20 Suitland, Maryland 20023	1
19.	Mr. Larry Ott Code 2022 Naval Air Development Center Johnsville, Warminster, Pennsylvania 18974	1
20.	Dr. Richard Honey Staff Scientist Stanford Research Institute Meno Park, California 94025	1
21.	Dr. Robert Fossum, Director DARPA 1400 Willson Blvd. Arlington, Virginia 22209	1

		No. Copies
22.	Asst. Professor S. P. Tucker, Code 68Tx Department of Oceanography Naval Postgraduate School Monterey, California 93940	1
23.	Assoc. Professor E. B. Thornton, Code 68Tm Department of Oceanography Naval Postgraduate School Monterey, California 93940	1
24.	Assoc. Professor R. N. Forrest, Code 55Fo Department of Operations Research Naval Postgraduate School Monterey, California 93940	1
25.	Dr. P. H. Moose, Code 61Me Department of Physics and Chemistry Naval Postgraduate School Monterey, California 93940	1
26.	Professor Otto Heinz, Code 61Hz Department of Physics and Chemistry Naval Postgraduate School Monterey, California 93940	1
27.	Peter McCardel, Code 52102 Naval Ocean Systems Center San Diego, California 92152	2
28.	Mr. B. Dillion, Code Air 370 Naval Air Systems Command Headquarters Washington, DC 20361	1
29.	Commander Patrol Wings, Atlantic Naval Air Station Brunswick, Maine 04011	1
30.	Commander Patrol Wings, Pacific Naval Air Station Moffett Field, California 94035	1
31.	Dean of Research, Code 012 Naval Postgraduate School Monterey, California 93940	1

Thesis
E723 Etro
c.1
80133
Production of ultra low frequency magnetic noise by ocean surface gravity waves and its real time removal from airborne magnetometer measurements.